

# Ensemble estimates of global wetland methane emissions over 2000-2020

Zhen Zhang<sup>1</sup>, Benjamin Poulter<sup>2</sup>, Joe R. Melton<sup>3</sup>, William J. Riley<sup>4</sup>, George H. Allen<sup>5</sup>, David J. Beerling<sup>6</sup>, Philippe Bousquet<sup>7</sup>, Josep G Canadell<sup>8</sup>, Etienne Fluet-Chouinard<sup>9</sup>, Philippe Ciais<sup>7</sup>, Nicola Gedney<sup>10</sup>, Peter O. Hopcroft<sup>11</sup>, Akihiko Ito<sup>12</sup>, Robert B. Jackson<sup>13</sup>, Atul K. Jain<sup>14</sup>, Katherine Jensen<sup>15</sup>, Fortunat Joos<sup>16</sup>, Thomas Kleinen<sup>17</sup>, Sara Knox<sup>18,19</sup>, Tingting Li<sup>20</sup>, Xin Li<sup>1</sup>, Xiangyu Liu<sup>21</sup>, Kyle McDonald<sup>15</sup>, Gavin McNicol<sup>22</sup>, Paul A. Miller<sup>23</sup>, Jurek Müller<sup>16</sup>, Prabir K. Patra<sup>24,25</sup>, Changhui Peng<sup>26</sup>, Shushi Peng<sup>27</sup>, Zhangcai Qin<sup>28</sup>, Ryan M. Riggs<sup>29</sup>, Marielle Saunois<sup>7</sup>, Qing Sun<sup>16</sup>, Hanqin Tian<sup>30</sup>, Xiaoming Xu<sup>14</sup>, Yuanzhi Yao<sup>31</sup>, Xi Yi<sup>27</sup>, Wenxin Zhang<sup>22</sup>, Qing Zhu<sup>4</sup>, Qiuhan Zhu<sup>32</sup>, Qianlai Zhuang<sup>21</sup>

10 <sup>1</sup>National Tibetan Plateau Data Center (TPDC), State Key Laboratory of Tibetan Plateau Earth System, Environment and Resource (TPESER), Institute of Tibetan Plateau Research, Chinese Academy of Sciences, Beijing, 100101, China

<sup>2</sup>NASA Goddard Space Flight Center, Earth Sciences Division, Greenbelt, MD, USA

<sup>3</sup>Climate Research Division, Environment and Climate Change Canada, Victoria, BC, Canada

<sup>4</sup>Climate and Ecosystem Sciences Division, Lawrence Berkeley National Laboratory, Berkeley, California, USA

15 <sup>5</sup>Department of Geosciences, Virginia Polytechnic Institute and State University, Blacksburg, VA, USA

<sup>6</sup>School of Biosciences, University of Sheffield, U.K.

<sup>7</sup>Laboratoire des Sciences du Climat et de l'Environnement, CEA, CNRS, UVSQ, universit& Paris-Saclay, Gif sur Yvette, France

<sup>8</sup>Global Carbon Project, CSIRO Environment, ACT 2601, Australia

20 <sup>9</sup>Earth Systems Science Division, Pacific Northwest National Laboratory, Richland, WA 99352, USA

<sup>10</sup>Met Office Hadley Centre, Joint Centre for Hydrometeorological Research, Wallingford, U.K.

<sup>11</sup>School of Geography, Earth & Environmental Sciences, University of Birmingham, U.K.

<sup>12</sup>National Institute for Environmental Studies, Tsukuba, Japan

25 <sup>13</sup>Department of Earth System Science, Woods Institute for the Environment, and Precourt Institute for Energy, Stanford University, Stanford, CA 94305-2210, USA

<sup>14</sup>Department of Atmospheric Sciences, University of Illinois, Urbana, IL 61821, USA

<sup>15</sup>Department of Earth and Atmospheric Sciences, City College of New York, City University of New York, NY, USA

<sup>16</sup>Climate and Environmental Physics, Physics Institute and Oeschger Centre for Climate Change Research, University of Bern

<sup>17</sup>Max Planck Institute for Meteorology, Hamburg, Germany

30 <sup>18</sup>The University of British Columbia, Vancouver, BC, Canada

<sup>19</sup>McGill University, Montreal, QC, Canada

<sup>20</sup>LAPC, Institute of Atmospheric Physics, Chinese Academy of Sciences, Beijing, 100029, China

<sup>21</sup>Department of Earth, Atmospheric, Planetary Sciences, Purdue University, West Lafayette, IN, USA

<sup>22</sup>Department of Atmospheric Sciences, University of Illinois, Chicago, IL, USA

35 <sup>23</sup>Department of Physical Geography and Ecosystem Science, Lund University, Sölvegatan 12, 223 62, Lund, Sweden

<sup>24</sup>Japan Agency for Marine-Earth Science and Technology (JAMSTEC), Yokohama, Japan

<sup>25</sup>Research Institute for Humanity and Nature (RIHN), Kyoto, Japan

<sup>26</sup>Department of Biology Sciences, University of Quebec at Montreal, C.P. 8888, Succ. Centre-Ville, Montreal, QC H3C 3P8, Canada

40 <sup>27</sup>Sino-French Institute for Earth System Science, Laboratory for Earth Surface Processes, College of Urban and Environmental Sciences, Peking University, Beijing 100871, China

<sup>28</sup>School of Atmospheric Sciences, Sun-Yat-Sen University, and Southern Marine Science and Engineering Guangdong Laboratory (Zhuhai), Zhuhai 519000, China

<sup>29</sup>Department of Geography, Texas A&M University, College Station, TX, USA

45 <sup>30</sup>Center for Earth System Science and Global Sustainability, Schiller Institute for Integrated Science and Society, Department of Earth and Environmental Sciences, Boston College, Chestnut Hill, MA 02467, USA

<sup>31</sup>School of Geographic Sciences, East China Normal University, Shanghai, China

<sup>32</sup>College of Hydrology and Water Resources, Hohai University, Nanjing, 210098, China

*Correspondence to: Zhen Zhang (yuisheng@email.com)*

50 **Abstract.** Due to ongoing climate change, methane (CH<sub>4</sub>) emissions from vegetated wetlands are projected to increase during  
the 21<sup>st</sup> century, challenging climate mitigation efforts aimed at limiting global warming. However, despite reports of rising  
emission trends, a comprehensive evaluation and attribution of recent changes remains limited. Here we assessed global  
wetland CH<sub>4</sub> emissions from 2000 to 2020 based on an ensemble of sixteen process-based wetland models. Our results  
55 estimated global average wetland CH<sub>4</sub> emissions at 158±24 (mean ± 1σ) Tg CH<sub>4</sub> yr<sup>-1</sup> over a total annual average wetland area  
of 8.0±2.0 Mkm<sup>2</sup> for the period 2010-2020, with an average increase of 6-7 Tg CH<sub>4</sub> yr<sup>-1</sup> in 2010-2019 compared to the average  
for 2000-2009. The increases in the four latitudinal bands of 90°S-30°S, 30°S- 30°N, 30°N-60°N, and 60°N-90°N were 0.1-  
0.2 Tg CH<sub>4</sub> yr<sup>-1</sup>, 3.6-3.7 Tg CH<sub>4</sub> yr<sup>-1</sup>, 1.8-2.4 Tg CH<sub>4</sub> yr<sup>-1</sup>, and 0.6-0.8 Tg CH<sub>4</sub> yr<sup>-1</sup>, respectively, over the two decades. The  
modeled CH<sub>4</sub> sensitivities to temperature show reasonable consistency with eddy covariance-based measurements from 34  
60 sites. Rising temperature was the primary driver of the increase, while precipitation and rising atmospheric CO<sub>2</sub> concentrations  
played secondary roles with high levels of uncertainty. These modeled results suggest climate change is driving increased  
wetland CH<sub>4</sub> emissions and that direct and sustained measurements are needed to monitor developments.

## 1 Introduction

Wetlands are the largest single source in the global methane (CH<sub>4</sub>) budget, representing ~25-35% of the total combined natural and anthropogenic sources (Kirschke et al., 2013; Saunio et al., 2016, 2020), with an uncertainty range of 100-230 Tg CH<sub>4</sub> yr<sup>-1</sup> (Cao et al., 1996; Gedney et al., 2004; Bousquet et al., 2006; Petrescu et al., 2010; Spahni et al., 2011; Melton et al., 2013; Bridgham et al., 2013; Bloom et al., 2017; Poulter et al., 2017). Covering 8-10% of the global land surface (Zhang et al., 2021a), wetland area is sensitive to climate variations (Zhang et al., 2018; Zhu et al., 2017). Over the last deglaciation, wetlands played an important role in driving the rise of atmospheric CH<sub>4</sub> concentrations (Hopcroft et al., 2017; Nisbet et al., 2023; Kleinen et al., 2023). In recent decades, wetlands have experienced unprecedented and ongoing changes, including continuous thawing of permafrost (Natali et al., 2019; Treat et al., 2018), land-use change (Fluet-Chouinard et al., 2023), a lengthening of the growing season in the Arctic (Arndt et al., 2019), and expansion in tropical areas due to enhanced precipitation (Fleischmann, 2023). Recent evidence from in situ measurements (Rößger et al., 2022), data driven estimates (Yuan et al., 2024; Ying et al., 2024), and satellite observations (Feng et al., 2022) suggests that these ongoing changes could enhance wetland CH<sub>4</sub> emissions and thus affect the trajectory of atmospheric CH<sub>4</sub> concentration. Furthermore, atmospheric δ<sup>13</sup>C-CH<sub>4</sub> records also show a trend toward increased depletion since the late 2000s (Lan et al., 2021; Nisbet et al., 2019), indicating that isotopically light biogenic sources, such as wetlands (Basu et al., 2022; Feng et al., 2022), agricultural, and waste sources (Schaefer et al., 2016; Zhang, et al., 2021b) have become dominant contributors to the rise in atmospheric CH<sub>4</sub>. Current estimates of wetland CH<sub>4</sub> emissions (hereafter denoted as eCH<sub>4</sub>) in response to climate change are projected to increase by up to 15-30% by 2050 (Koffi et al., 2020; Zhang et al., 2017), accounting for 25-40% of the pledged reduction in anthropogenic emissions (Shindell et al., 2019). These trends and projections suggest that the emerging wetland-CH<sub>4</sub> climate feedback that influences atmospheric CH<sub>4</sub> concentration requires a better understanding of long-term changes in eCH<sub>4</sub>.

Directly diagnosing the variations and trends of eCH<sub>4</sub> at large scales is challenging. Site-level measurements, such as those from chamber and eddy covariance techniques, are useful for identifying underlying mechanisms and monitoring CH<sub>4</sub> fluxes at the landscape scale but are difficult to upscale due to large uncertainties in extrapolation and the high spatial heterogeneity of wetland CH<sub>4</sub> fluxes (Chu et al., 2021; Kuhn et al., 2021). Interpreting eCH<sub>4</sub> using satellite observations and inversions of atmospheric concentration data is also subject to uncertainties in anthropogenic sources, other natural sources, atmospheric chemistry, and model errors associated with atmospheric transport (Gatti et al., 2021; Gloor et al., 2021; Palmer et al., 2022; Patra et al., 2011; Zhang et al., 2021c). Global wetland models, integrated within land biosphere models, can serve to bridge our understanding of wetland CH<sub>4</sub> processes and diagnosing wetland CH<sub>4</sub> dynamics at large scales (Melton et al., 2013; Wania et al., 2013). These models provide mechanistic explanations for the causes of changes in eCH<sub>4</sub> dynamics. Furthermore, recent advances in wetland models (Arora et al., 2018; Kaiser et al., 2017; Shu et al., 2020; Grant 2017; Chang et al. 2020) show significant potential for improving our understanding of eCH<sub>4</sub> through the incorporation of complex biogeochemical processes.

95 Current studies have reached various conclusions on the change in eCH<sub>4</sub> over the last decades. Studies based on single biogeochemical models (Zhang et al., 2018; Zhu et al., 2017) suggest a significant increase in eCH<sub>4</sub> from 2000-2006 to 2007-2017, while atmospheric inversions (Zhang et al., 2021c; Yin et al., 2021; Basu et al., 2022; Feng et al., 2022) suggested even higher rate increases, from 2 Tg CH<sub>4</sub> yr<sup>-1</sup> yr<sup>-1</sup> to 3 Tg CH<sub>4</sub> yr<sup>-1</sup> yr<sup>-1</sup> during the post-2010 period. Poulter et al., (2017) reported no significant change between the 2000-2006 and 2007-2012 periods based on an ensemble of wetland models, while Saunio et al. (2020) show a slight increase (~2 Tg CH<sub>4</sub> yr<sup>-1</sup>) in average for 2007-2017 compared to the 2000-2006 level using a large set of wetland CH<sub>4</sub> models. However, these models demonstrate considerable differences in estimated eCH<sub>4</sub>, both spatially and temporally (Ma et al., 2021; Parker et al., 2020; Chang et al., 2023), primarily due to the sensitivity of their estimations to the wetland areal extent, the implemented biogeochemical structures, and parameterizations. The multi-model ensemble approach is applied to increase the skill, reliability, and consistency of model forecasts, potentially offsetting individual model errors (Schaefer et al., 2012). However, a recent study (Chang et al. 2023) found that down selecting atmospheric inversion and wetland model CH<sub>4</sub> predictions based on a comparison to eddy covariance data did not reduce uncertainty in global eCH<sub>4</sub> estimates. Therefore, it has become necessary to thoroughly evaluate the performance of these models using the most recent generation of wetland models against an increasingly dense network of observations (Delwiche et al., 2021; Knox et al., 2019) from eddy covariance sites.

110

Here we conducted ensemble simulations of 16 wetland biogeochemical models following a common modeling protocol to provide monthly integrated global eCH<sub>4</sub> for the period of 2000-2020, as part of the Global Carbon Project's Methane Budget activity. The inundation dynamics of each model were simulated using a model-specific prognostic hydrological modeling approach as well as a set of diagnostic satellite-driven simulations. A set of factorial simulations were carried out to isolate the effects of temperature, precipitation, and rising atmospheric CO<sub>2</sub> concentration. The modeled temperature sensitivity was evaluated against the global eddy covariance database, FLUXNET-CH<sub>4</sub> (Delwiche et al., 2021; Knox et al., 2019), and a data-driven global wetland CH<sub>4</sub> upscaling dataset UpCH<sub>4</sub> (McNicol et al., 2023) based on FLUXNET-CH<sub>4</sub>. In addition, we examined the changes in eCH<sub>4</sub> for the year 2020, which was characterized as an extremely warm and wet year with the highest growth rate of atmospheric CH<sub>4</sub> observed over the study period.

120

## 2 Methods

### 2.1 Wetland model ensemble

Sixteen wetland models participated in the ensemble simulations (Table S1). Wetland CH<sub>4</sub> models can be generally described as functions describing the biogeochemical processes that control CH<sub>4</sub> production and oxidation through methanogenesis and methanotrophy, and the biophysical processes that regulate CH<sub>4</sub> transport from the soil to the atmosphere (Table S1). Methanogenesis in the models is linked to different proxies (e.g., carbon substrate, heterotrophic respiration, net primary

125

production) with a wide range of model complexity - more sophisticated models include wetland Plant Functional Types (PFTs) and explicitly simulate the processes of CH<sub>4</sub> production, consumption, and transport, while the simplified models use generalized empirical equations to simulate net fluxes without explicitly calculating individual components of the CH<sub>4</sub> flux.

130

Wetlands were defined as naturally vegetated forested and non-forested ecosystems with saturated/inundated areas, excluding coastal wetlands, cultivated wetlands such as rice paddies, and open water systems such as rivers, lakes, ponds, and reservoirs. A prognostic wetland inundation scheme and a diagnostic wetland dataset Wetland Area and Dynamics for Methane Modeling (WAD2M v2; Zhang et al., 2021a) are applied to identify the wetland areal dynamics. The prognostic wetland areal dynamics were independently determined by each model's hydrological modules, which use water table depth or soil moisture, combined with sub-grid topographic conditions to determine saturated areas within a land surface grid-cell (Zhang et al., 2016; Xi et al., 2022). Among the participating models, there was a large variation in complexity and in the level of comprehensiveness with which wetland extent were characterized. The modules for simulating inundation ranged from simplified TOPMODEL approaches to more sophisticated representations of water-table variation, with the estimated magnitude being influenced by the hydrologic schemes utilized and the sensitivities to precipitation. The prognostic modeled wetland extent showed large variability in estimated magnitude but was consistent with satellite-based inundation products in predicting different phases of inundation (Xi et al., 2022; Zhang, et al., 2021a). The ensemble mean of the modeled wetland extent is close to 7.5 Mkm<sup>2</sup> as estimated by WAD2M but higher than the 4.6 Mkm<sup>2</sup> by the satellite-based product Global Surface Water Extent and Dynamics version 2 (GIEMS2; Prigent et al., 2020). The modeled temporal variations in wetland areas have high correlations with the satellite-based products for the temperate region and high latitudes (Fig. S1), except for the tropics. The modeled temporal variations in wetland areas show high correlations with satellite-based products for temperate regions and high latitudes (Fig. S1), except in the tropics. The limited agreement in the tropics may be due to the influence of aerosols and clouds on satellite-based measurements, as well as the process-based model's performance limitations in representing wetland areas. The diagnostic runs are exclusively used for temperature dependence calculations due to a discontinuity issue in the WAD2Mv2 over a few tropical hotspots, which affect a subset of wetland models that are particularly sensitive to inundation in the hotspots.

145

150

## 2.2 Modeling protocol and simulation setups

The modeling protocol aimed to provide wetland CH<sub>4</sub> fluxes and quantify the associated uncertainties arising from model differences, meteorological forcing, and wetland extent dynamics. To quantify meteorological forcing uncertainty, we used two climate inputs, a ground-based monthly climate dataset from the Climatic Research Unit (CRU) (Harris et al., 2014), up to 2020 and a harmonized daily dataset from the Global Soil Wetness Project-3 GSWP3-W5E5 through the year 2019, which is a multiple-source-based daily dataset (Cucchi et al., 2020; Dirmeyer et al., 2006) used in the Inter-Sectoral Impact Model Intercomparison Project 3a (ISIMIP3a). For models that require 6-hourly meteorological forcings, a temporal-interpolation dataset CRU-JRA was applied based on the Japanese Reanalysis Agency (JRA55), aligned with CRU. The atmospheric CO<sub>2</sub> concentration values for 1861-2020 were obtained from the CMIP6 experimental protocol (Meinshausen et al., 2017).

155

160 Ancillary data, such as soil texture and CH<sub>4</sub>-related parameter sets used model-specific inputs. All the models were run in  
'natural vegetation' mode without transient effects of land use and land cover change. Methane oxidation in wetland soils was  
implicitly included in the estimate but the upland oxidative sink was not included as it was not part of the net wetland emissions  
calculations. Models included the spin-up period to pre-industrial conditions assuming net ecosystem exchange equilibrium  
before 1860 by recycling fixed CO<sub>2</sub> concentrations (1860 level of 286.42 ppm) and meteorology (1901-1920).

### 165 **2.3 FLUXNET-CH<sub>4</sub> and machine learning-based upscaling product UpCH<sub>4</sub>**

FLUXNET-CH<sub>4</sub> is the first global dataset of CH<sub>4</sub> eddy covariance measurements that includes ~ 80 sites globally, including  
different wetland types from peatlands (e.g. bog, fen), mineral wetlands (e.g. marsh, swamp), and rice paddies. For this study,  
a subset of natural freshwater wetland sites was selected for the analysis. All the eddy covariance measurements used in this  
study were gap-filled daily total fluxes filled using an Artificial Neural Network (ANN) approach (Knox et al., 2019). In  
170 addition, a data-driven gridded dataset UpCH<sub>4</sub> (McNicol et al., 2023) for 2001-2018, which is based on 119 site-years of CH<sub>4</sub>  
fluxes from the FLUXNET-CH<sub>4</sub> dataset, was applied in the comparison. This dataset used a random forest model to upscale  
ground-based eddy covariance CH<sub>4</sub> flux data and then was forced with globally-gridded predictor data and two wetland extent  
products, to predict wetland CH<sub>4</sub> emissions. The predictors included data sources from climate, biometeorological, and soil  
properties.

### 175 **2.4 Time series decomposition and statistical analyses**

To attribute the time series of global wetland CH<sub>4</sub> emissions to what we consider the dominant drivers of change (i.e.,  
temperature, precipitation, and CO<sub>2</sub> concentration), we applied a multiple regression approach (Piao et al., 2013) to estimate  
the parameters of global wetland CH<sub>4</sub> sensitivity to climate drivers using the following equation:

$$y = \beta CO_2 + \gamma Tmp + \delta Pre + c + \varepsilon \quad (1)$$

180 where  $y$  is the global annual total wetland CH<sub>4</sub> emission of each model from the transient run, or from the observation-based  
upscaling dataset UpCH<sub>4</sub>, and  $Tmp$ ,  $Pre$ , and  $CO_2$  are the mean annual temperature, total annual precipitation, and mean  
atmospheric CO<sub>2</sub> concentration for that year, respectively.  $\gamma$ ,  $\delta$ ,  $\beta$ , and  $c$  are regression coefficients and  $\varepsilon$  is the residual error  
term. The regression coefficients were calculated using a maximum likelihood estimate. Changes in other meteorological  
forcings may also influence the estimation of  $y$ . These confounding drivers, such as solar radiation and wind speed, although  
185 they are considered to have minor impacts on the variations of  $eCH_4$ , were implicitly accounted for in the regression  
coefficients.

### **2.5 Model factorial experiment**

To further separate the contribution of different controls on the change in methane emissions ( $\Delta eCH_4$ ) by climate variations  
and rising CO<sub>2</sub>, we used a subset of four models that conducted factorial experimental simulations by holding each factor

190 constant during part of the transient runs. This subset of the wetland models (i.e., ELM-ECA, LPJ-wsl, SDGVM, and VISIT) performed a set of factorial simulations to specifically attribute the effect of temperature, precipitation, and rising CO<sub>2</sub> concentration on wetland CH<sub>4</sub> fluxes with the climatology of 2000-2006 for 2007-2020. The simulations were performed by running the model keeping one-factor constant at a time to estimate the contribution of each component to the total range of variations (Table S2). For these factorial simulations, we evaluated the annual amplitude of wetland eCH<sub>4</sub> as a relative  
195 percentage change to minimize the impacts of different modeling implementation choices, such as different input variables among models. The effect of the total changes on the relative change in amplitude was represented by the difference between the transient (one factor is time-varying) and baseline (static at 2000-2006 levels) runs. For simplicity, the relative contribution of a single driver to eCH<sub>4</sub> variations was quantified as the transient run minus the specific control run. To calculate the contribution of each driver using the subset of the models, we calculated weighting factors per year across the models, with  
200 lower bias resulting in higher weight relative to the full ensemble mean using an inverse function.

## 2.6 Temperature dependence calculation

To further evaluate the response of eCH<sub>4</sub> to rising temperatures, we calculated the modeled seasonal eCH<sub>4</sub> temperature dependence, referred to as the apparent Q<sub>10</sub> metric at the locations of 34 FLUXNET-CH<sub>4</sub> sites. This seasonal Q<sub>10</sub> differs from the intrinsic Q<sub>10</sub> prescribed in the parameterization of respiratory processes in each model. Here it represents the overall  
205 response of eCH<sub>4</sub> along geographic temperature gradients. The apparent Q<sub>10</sub> is defined as eCH<sub>4</sub> sensitivity to temperature change. We calculated apparent Q<sub>10</sub> based on CH<sub>4</sub> emitting strength over a standard wetland area, which was calculated as the CH<sub>4</sub> fluxes divided by inundated area on a per-pixel basis to exclude the effect of inundation dynamics. To derive the temperature sensitivity of eCH<sub>4</sub> at the soil or ecosystem level, we applied the following equation:

$$R(i) = R_b(i)Q_{10}^{\frac{T(i) - T_{ref}}{F}} \quad (2)$$

210 where R(i) is the net wetland flux at the location of site *i*, R<sub>b</sub>(i) is the basal net CH<sub>4</sub> flux at the reference temperature T<sub>ref</sub>, and T(i) is ambient temperature. The parameters Q<sub>10</sub>, F= 10°C, and T<sub>ref</sub>= 15°C are all time-independent constants. The Q<sub>10</sub> acting on specific time scales can be obtained from eCH<sub>4</sub> at corresponding specific time scales (i.e., seasonal total and annual total) by fitting an exponential regression with modeled eCH<sub>4</sub> and air temperature from CRU or GSWP3-W5E5. To quantify the uncertainty in observed apparent Q<sub>10</sub>, we employed 1000 sets of resampled FLUXNET-CH<sub>4</sub> observations generated based on  
215 a Gaussian distribution. The uncertainty range in measured seasonal mean CH<sub>4</sub> fluxes was determined by aggregating the uncertainty of daily total fluxes obtained through ANN gap filling.

### 3 Results and Discussion

#### 3.1 Changes in eCH<sub>4</sub> during the period of 2000-2020

The multi-model ensemble based on the prognostic inundation schemes shows that the average annual global eCH<sub>4</sub> over the period 2000-2020 was  $156 \pm 24$  Tg CH<sub>4</sub> yr<sup>-1</sup> (mean  $\pm 1\sigma$ ). The average annual eCH<sub>4</sub> increased from  $153 \pm 23$  Tg CH<sub>4</sub> yr<sup>-1</sup> during 2000-2009 to  $158 \pm 24$  Tg CH<sub>4</sub> yr<sup>-1</sup> during 2010-2020. 15 out of 22 model simulations show significant positive linear trends ( $p < 0.01$ ) with an ensemble mean increase rate of  $0.6 \pm 0.3$  Tg CH<sub>4</sub> yr<sup>-1</sup> yr<sup>-1</sup> over 2000-2020 (Fig. 1a; Table 1; Fig. S2). Differences in total annual emissions between the two sets of simulations driven by two different climate datasets CRU and GSWP3-W5E5, agree well in the magnitude of the annual anomalies. Notable eCH<sub>4</sub> variations to climate events were observed, such as the rise during the 2010 La Niña ( $+5.2$  Tg CH<sub>4</sub> yr<sup>-1</sup>) and the decline during the 2015 El Niño ( $-4.6$  Tg CH<sub>4</sub> yr<sup>-1</sup>) after removing the positive linear trends. The multi-model ensemble wetland eCH<sub>4</sub> response to climate events is consistent with those reported by earlier studies (Zhang et al., 2018; Zhu et al., 2017) using single wetland models, indicating a modulation of the phase of eCH<sub>4</sub> anomaly ( $\Delta eCH_4$ ) by the El Niño-Southern Oscillation. The model ensemble demonstrates a consistent increase in interannual variability (IAV) in  $\Delta eCH_4$  from  $3.6 \pm 1.6$  Tg CH<sub>4</sub> yr<sup>-1</sup> during 2000-2009 to  $4.7 \pm 1.5$  Tg CH<sub>4</sub> yr<sup>-1</sup> during 2010-2020, suggesting a potential increase in eCH<sub>4</sub> variability under climate change.

The models consistently show that 2020 is the strongest positive anomaly year during 2000-2020, with a net increase of 2 [-2, 7] Tg CH<sub>4</sub> yr<sup>-1</sup> (mean [min, max]) in 2020 compared to 2019. This positive anomaly in 2020 (Table 1) is broadly consistent with a recent study (Peng et al., 2022) that reported  $6 \pm 2.3$  Tg CH<sub>4</sub> yr<sup>-1</sup> based on simulations of two bottom-up models with different climate datasets. The discrepancy in estimated magnitude between the Peng et al. (2022) and our results are partly due to the parameterizations of CH<sub>4</sub> module that causes lower annual magnitude in this study ( $\sim 162 \pm 23$  Tg CH<sub>4</sub> yr<sup>-1</sup> in 2020) compared to the Peng et al. (2022) study ( $177 \pm 31$  Tg CH<sub>4</sub> yr<sup>-1</sup> in 2020). Additionally, the precipitation inputs in the climate forcing used in this study show a lower positive anomaly ( $\sim$  of 20 mm yr<sup>-1</sup> in CRU over global wetland) in precipitation in 2020 compared to the reanalysis-based estimates ( $\sim 40$ -117 mm yr<sup>-1</sup> over global wetland used in the study by Peng et al., (2022), which leads to lower estimates of wetland area and consequently lower emissions in this study. Moreover, our model ensemble does not indicate a strong increase ( $-0.2$ [-1.5-0.7] Tg CH<sub>4</sub> yr<sup>-1</sup>) in eCH<sub>4</sub> in Africa in 2020. This contrasts with recent atmospheric inversions (Feng et al., 2023; Qu et al., 2023), which suggest a large increase of 11-17 Tg CH<sub>4</sub> yr<sup>-1</sup> above 2019 levels in African CH<sub>4</sub> emissions for 2020. The estimated increase from these inversions is equivalent to 55%-85% of total eCH<sub>4</sub> in Africa during 2010-2019 in our study (Figure 2). These discrepancies highlight the need for further studies to investigate the differences between these two approaches, including uncertainty in climate inputs in process-based bottom-up models and partitioning difference sources in atmospheric inversions.



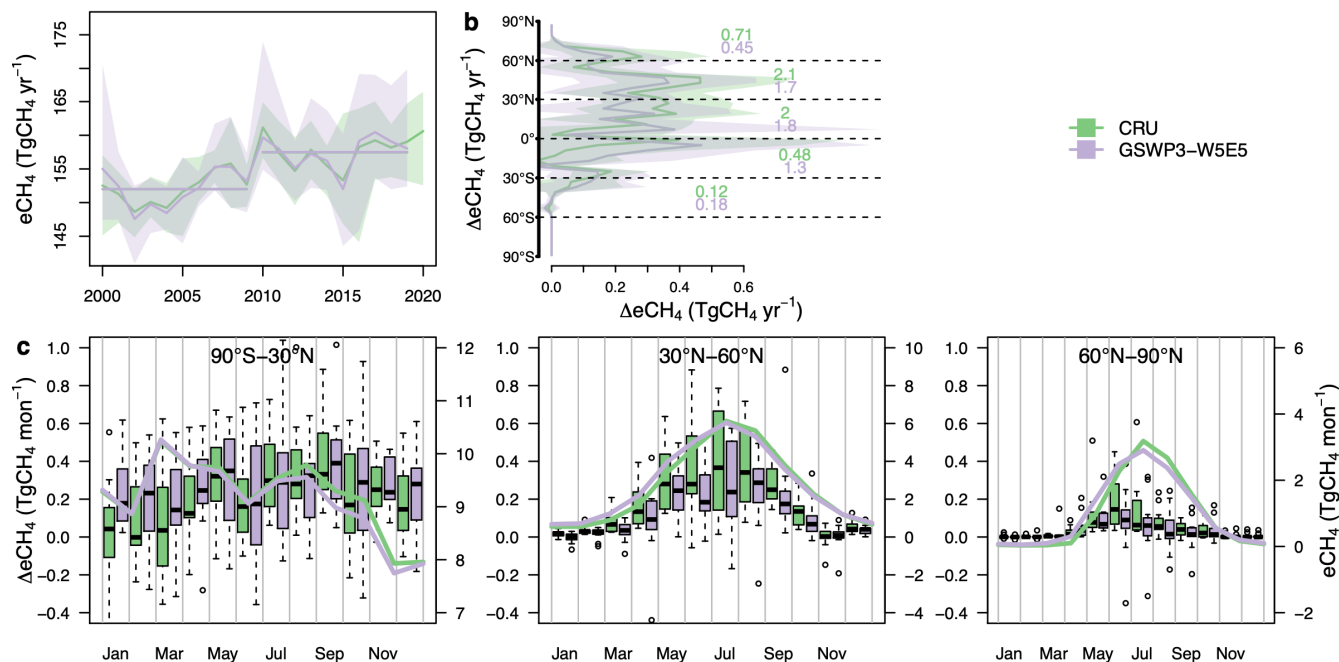


**Figure 1: Simulated global wetland CH<sub>4</sub> emissions from the model ensemble for 2000-2020.** a, Time series of annual total emissions during 2000-2020, with the shaded area representing the range between minimum and maximum modeled emissions. The horizontal lines represent the ensemble means of 2000-2009 (152 Tg CH<sub>4</sub> yr<sup>-1</sup>) and 2010-2019 (158 Tg CH<sub>4</sub> yr<sup>-1</sup>), respectively. b, Latitudinal gradient of eCH<sub>4</sub> difference ( $\Delta e\text{CH}_4$ ), with the mean annual total  $\Delta e\text{CH}_4$  for each of the 30° latitude bins from the two sets of simulations shown. The change is calculated relative to the mean of the 2000-2009 level from the two sets of simulations with prognostic wetland emission models grouped by different climate datasets, CRU and GSWP3-W5E5. c, Boxplots of mean seasonal  $\Delta e\text{CH}_4$  for the three regions. The central mark and the bottom and top edges of the box indicate the median, and the 25th and 75th percentiles of the ensemble, respectively. The colored lines represent the average seasonal cycle of 2000-2009 from the simulations grouped by two climate datasets, CRU and GSWP3-W5E5.

There were widespread net increases in eCH<sub>4</sub> across all latitudinal bands during 2010-2020, compared to the average of 2000-2009, with the largest magnitudes occurring in the 90°S- 30°N bands (there are relatively few wetlands in the southern extratropics 90°S-30°S, contributing 0.1-0.2 Tg CH<sub>4</sub> yr<sup>-1</sup>) and temperate regions (30-60°N) (Fig. 1b). The annual magnitude of eCH<sub>4</sub> increased by 3.7-3.8 Tg CH<sub>4</sub> yr<sup>-1</sup>, 1.8-2.4 Tg CH<sub>4</sub> yr<sup>-1</sup>, and 0.6-0.8 Tg CH<sub>4</sub> yr<sup>-1</sup> in the tropical, temperate, and Arctic wetlands, respectively. The tropics have experienced the largest increases in annual total emissions with an increase of 3% relative to 2000-2009 (Table 1). This finding is aligned with the results of several recent atmospheric inversions (Basu et al., 2022; Feng et al., 2022; Lan et al., 2021) using satellite observations and/or isotopic measurements that suggest a large increase in microbial emissions for post-2007 period in the tropics. While the increase in annual total emissions from temperate wetlands is lower than that from the tropics, they nevertheless show a larger relative increase of 5-8% compared to 2000-2009. Arctic wetlands also show an increased rate of 5-7% relative to the same period.

The increase in eCH<sub>4</sub> occurs in parallel with differing patterns of enhanced seasonal cycles between tropical and extratropical wetlands (30°N-90°N) (Fig. 1c). In temperate and Arctic wetlands, the majority of the increase in emissions (60-92%) occurred

270 primarily during the growing season (May-October). Specifically, increases in Arctic wetlands occurred during the early  
growing season (May-July), aligning with findings from a data-driven estimate (Yuan et al., 2024) and a long-term eddy  
covariance-based study (Rößger et al., 2022) that observed early growing season increases in eCH<sub>4</sub> due to continuous warming  
in a Siberian wetland. In contrast, the increase in emissions within the 90°S-30°N band exhibited relatively minor seasonal  
275 variations throughout the year, with the May-October period accounting for a 24% greater increase in ΔeCH<sub>4</sub> compared to the  
November-April period (Fig. S3).

**Table 1. Summary of wetland CH<sub>4</sub> emissions (Tg CH<sub>4</sub> yr<sup>-1</sup>) over different time periods by latitudinal bands for the prognostic wetland simulations.** The ensemble mean with minimum and maximum (numbers within brackets) are listed, respectively.

Time period	Forcing	90°S-30°S	30°S-30°N	30°N-60°N	60°N-90°N	Global
2000-2009	CRU	3[1-5]	107[63-141]	31[16-60]	11[4-29]	152[119-187]
	GSWP3-W5E5	3[1-5]	106[60-142]	33[18-57]	11[4-29]	153[116-188]
2010-2019	CRU	3[1-6]	110[67-144]	34[17-64]	12[4-30]	158[126-193]
	GSWP3-W5E5	3[1-6]	110[64-146]	35[18-60]	12[4-29]	158[118-203]

### 3.2 Spatial distribution of eCH<sub>4</sub>

280 A few key regions contribute significantly to global emissions (Fig. 2a,c). These regions are mainly floodplains located along  
major river basins such as the Amazon, Ganges, Mississippi, and Yangtze; tropical peatlands in the Congo and Southeastern  
Asia; and high-latitude peatlands in the Hudson Bay Lowland (HBL) and West Siberian Lowland (WSL). However, inter-  
model variabilities in eCH<sub>4</sub> reveal varying levels of spatial agreement between models, with the largest discrepancies coming  
from South America and Africa. South America is one of the largest contributors to the global total eCH<sub>4</sub>. Still, the net change  
285 in that region shows only a moderate increase, with diverging trends within the Amazon basin during the 2010s (Fig. 2b,d).  
The uncertain temporal trends are consistent with a long-term, large-scale atmospheric inversion based on airborne campaigns  
(Basso et al., 2021). South Asia and Africa are among the regions with the largest increases in the tropics, next to North  
America, but have high uncertainty with a lower level of agreement among the models (Fig. S4). The model ensemble shows  
that Northwestern South Asia has a significant percentage increase in eCH<sub>4</sub> during 2010-2019 relative to its average levels  
290 from 2000-2009, suggesting a possible high sensitivity of eCH<sub>4</sub> to climate change in this region.

The comparison with previous estimates from bottom-up approaches and top-down atmospheric inversions (Table S3) suggests that the model ensemble mean generally captures well the spatial distribution of annual eCH<sub>4</sub>, with a potential underestimation for a few methane hotspots (Fig. S5). The model ensemble means for the Amazon basin, HBL, and WSL show good agreement with atmospheric inversions (Bergamaschi et al., 2013; Pickett-Heaps et al., 2011; Ringeval et al., 2014; Tunnicliffe et al., 2020; Wilson et al., 2016, 2021) and bottom-up modeling estimates (Bansal et al., 2023; Bloom et al., 2017; Bohn et al., 2015), with relatively low uncertainty. The model ensemble highlights WSL and HBL as CH<sub>4</sub> hotspots in the high latitudes, with good agreements of annual magnitudes with atmospheric inversions and in situ observations (Bohn et al., 2015; Glagolev et al., 2011; Pickett-Heaps et al., 2011), while the models have lower estimates for Alaska compared to the inversions (Chang et al., 2014; Miller et al., 2016). However, for the two hotspots of the Pantanal and Sudd wetlands, the models tended to underestimate the annual eCH<sub>4</sub> compared to a few recent satellite-based estimates (Gerlein-Safdi et al., 2021; Gloor et al., 2021; Lunt et al., 2021; Pandey et al., 2021), with a large uncertainty range of up to two orders of magnitude across the model ensemble (Fig. S5). In addition to the regions where eCH<sub>4</sub> are being underestimated, recent studies (France et al., 2022; Shaw et al., 2022) based on aircraft measurements suggest that the bottom-up models likely underestimate high eCH<sub>4</sub> fluxes in some little-studied wetlands, such as those in Zambia and Bolivia. The underestimations by process-based wetland models can be attributed to: 1) the challenge in accurately capturing the areal dynamics of wetlands under varying hydrological conditions, such as in flat terrains that receives lateral transport of water from upper streams (Li et al., 2024; Lunt et al., 2021; Gerlein-Safdi et al., 2021); 2) existing knowledge gaps in mapping wetlands in remote areas, which affect the parameterization of inundation modeling; 3) the limited representation of water table regulation (Chen et al., 2021) and wetland PFTs (Bastviken et al., 2023) on eCH<sub>4</sub> in biogeochemical models.

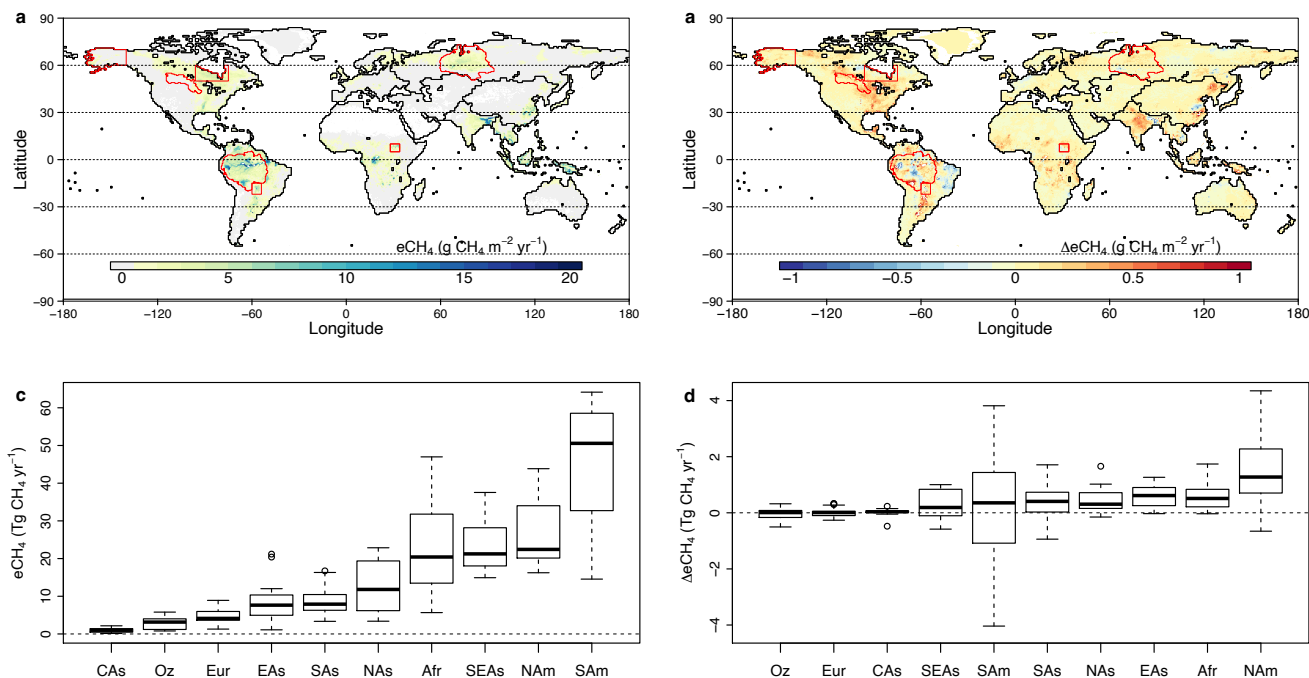


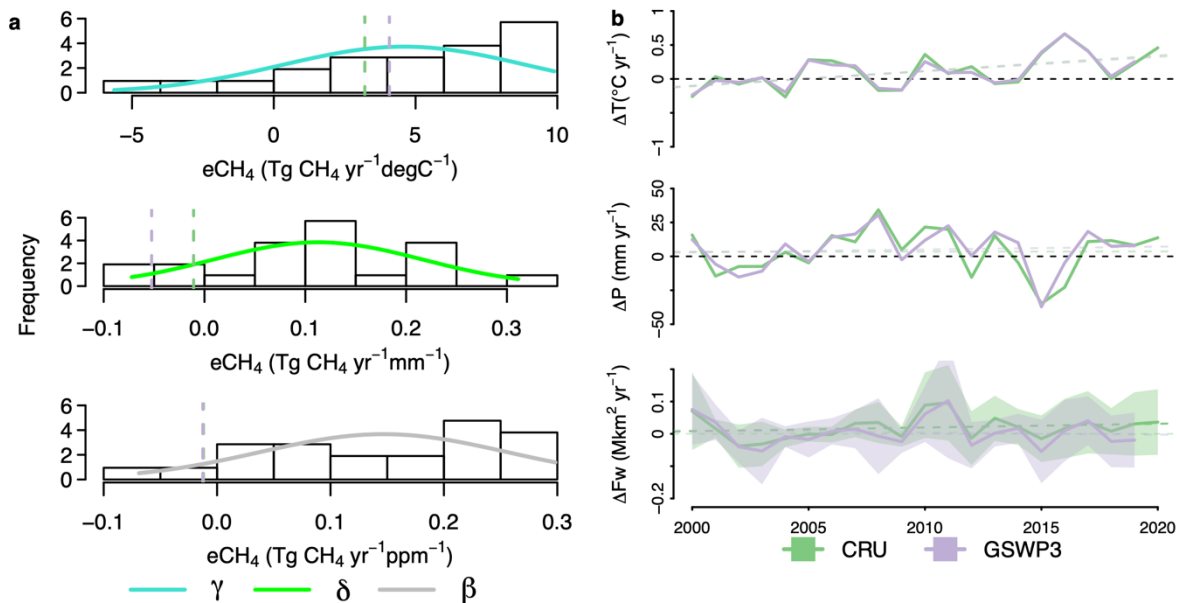
**Figure 2. Spatial distribution of eCH<sub>4</sub> and the average change between the 2010s and 2000s.** a. Map of mean eCH<sub>4</sub> (Unit: gCH<sub>4</sub> m<sup>-2</sup> yr<sup>-1</sup> per 0.5 deg grid cell) for 2000-2020. The regions defined in c, d and regional CH<sub>4</sub> hotspots in Table S3 are outlined in black and in red, respectively. b. Map of change in mean annual wetland emissions ( $\Delta$ eCH<sub>4</sub>) between the 2010s and 2000s. c. Boxplot of mean annual eCH<sub>4</sub> and d.  $\Delta$ eCH<sub>4</sub> by regions for 2000-2020 in ascending order for median estimates, Afr: Africa; CAs: Central Asia; EAs: East Asia; Eur: Europe; NAm: North America; NAs: North Asia; Oz: Oceania; SAM: South America; SAs: South Asia; SEAs: Southeast Asia.

### 3.3 Attribution of wetland CH<sub>4</sub> changes

To evaluate the relative contribution of different factors on global eCH<sub>4</sub>, we calculated the sensitivity of eCH<sub>4</sub> to mean annual temperature (denoted as  $\gamma$ ), annual total precipitation (denoted as  $\delta$ ), and CO<sub>2</sub> concentration (denoted as  $\beta$ ) using a multiple regression approach for each model run over the period of 2000-2020. The same approach was applied to the upscaled gridded machine learning dataset UpCH<sub>4</sub>, which uses eddy covariance measurements from FLUXNET-CH<sub>4</sub> as training inputs. The model ensemble suggests that temperature is the primary driver of the increase in eCH<sub>4</sub> (Fig. 3a). The regression coefficients for  $\gamma$  is 4.6 Tg CH<sub>4</sub> yr<sup>-1</sup> °C<sup>-1</sup>, with a range of -0.4 and 9.0 Tg CH<sub>4</sub> yr<sup>-1</sup> °C<sup>-1</sup> between the 10<sup>th</sup> and 90<sup>th</sup> percentiles among all models. This mean temperature sensitivity is slightly higher than the  $\gamma$  coefficient of 3.2-4.1 Tg CH<sub>4</sub> yr<sup>-1</sup> °C<sup>-1</sup> estimated for UpCH<sub>4</sub>. In contrast, precipitation contributed little to the increase from the prognostic simulations, with a coefficient  $\delta$  of 0 to 0.3 Tg CH<sub>4</sub> yr<sup>-1</sup> mm<sup>-1</sup>. The coefficient  $\delta$  was lower at -0.05-0 Tg CH<sub>4</sub> yr<sup>-1</sup> mm<sup>-1</sup> for UpCH<sub>4</sub>, as precipitation was not chosen as a model training predictor through its feature selection, based on site-level eddy covariance measurements (McNicol et al., 2023). However, precipitation is a more dominant factor at large scales, especially for tropical floodplains, which contribute the largest proportion of emissions but are poorly represented by eddy covariance measurements. The model ensemble estimated  $\beta$  remains small, ranging from 0 to 0.3 Tg CH<sub>4</sub> yr<sup>-1</sup> ppm<sup>-1</sup>, while UpCH<sub>4</sub> suggests a  $\beta$  at -0.01 Tg CH<sub>4</sub> yr<sup>-1</sup> ppm<sup>-1</sup>. However, other confounding drivers might influence eCH<sub>4</sub> as well, such as solar radiation, wind speed, and nitrogen deposition. Thus, the inferred sensitivities are implicitly accounted for in the regression coefficients despite their relatively small impacts compared to the major drivers.

Generally, the factorial simulations of the four-model subset indicated a consistently positive contribution (three out of four) from rising temperature to  $\Delta$ eCH<sub>4</sub>, with a large variability (s.d.=4.3 Tg CH<sub>4</sub> yr<sup>-1</sup>) of contributions from precipitation (Fig. S6). The strength of the CO<sub>2</sub> fertilization effect varied among models and was moderate but positive in all models. Two models (ELM-ECA and SDGVM) were among the models with higher sensitivity to climate variations while LPJ-wsl and VISIT were close to the full ensemble mean. ELM-ECA produced a negative temperature effect on eCH<sub>4</sub>, likely due to its modeled nutrient constraints and higher temperature sensitivity for methanotrophic compared to methanogenic processes. Considering the deviation of each model from the full ensemble mean, the weighted mean (Fig. S7) contributions for temperature, precipitation, and CO<sub>2</sub> concentration from the subset models were 3.2, 1.8, and 1.4 Tg CH<sub>4</sub> yr<sup>-1</sup>, respectively. The results from the subset of the models consistently demonstrate that temperature is the primary factor influencing eCH<sub>4</sub>.

Overall, the interannual variations of modeled eCH<sub>4</sub> were primarily associated with rising temperature, altered precipitation patterns, and rising atmospheric CO<sub>2</sub> concentrations that stimulated ecosystem productivity through the CO<sub>2</sub> fertilization effect (Yvon-Durocher et al., 2014). We note that a recent study found strong hysteresis in the seasonal temperature dependence of observed eCH<sub>4</sub> using the FLUXNET-CH<sub>4</sub> dataset (Chang et al. 2021). Those hysteretic features likely result in uncertainty in annual temperature sensitivity estimates but would not bias the conclusion of temperature as a dominant controller of eCH<sub>4</sub> at the decadal time scale. The links between rising temperature and enhanced net CH<sub>4</sub> fluxes are evident (as described below), as the annual global average temperature over wetland areas has significantly ( $p < 0.01$ ) increased by 0.5-0.7 °C from 2000-2020 (Fig. 3b). The modeled interannual variations of wetland extent dynamics reproduced the response to strong climate events (e.g., positive anomaly during the La Niña phase in 2010/2011 (Boening et al., 2012) and 2020). Both climate-forcing datasets suggest no significant trend in the anomaly of annual mean wetland area globally over the same period based on the prognostic hydrological simulations (Fig. 3b). Similarly, no significant regional trends in wetland area were found for most of the sub-regions, with the exception of South America, which shows a decrease, and East Asia, which shows a slight increase (Fig. S8). Considering that the extent of modeled wetland areas is primarily driven by precipitation, we do not detect a substantial contribution of changes in wetland extent to the long-term increase in eCH<sub>4</sub> over 2000-2020 based on the climate datasets. However, considerable differences in annual and seasonal precipitation estimates between the climate datasets used in this study and those derived from reanalysis or satellite-based products (Zhang et al., 2023a) result in large uncertainties in the estimated trends in wetland extent.



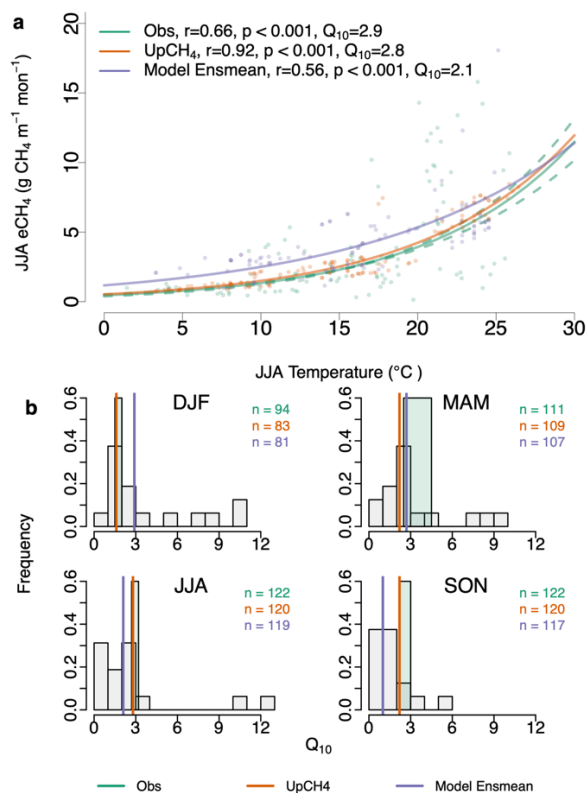
365 **Figure 3. Attributions of  $\Delta e\text{CH}_4$  during 2000-2020.** a. Histogram showing the sensitivity coefficients derived from a multiple regression  
approach (See Methods) for temperature ( $\gamma$ ), precipitation ( $\delta$ ), and atmospheric  $\text{CO}_2$  concentration ( $\beta$ ). The curves represent probability  
distributions of sensitivity coefficients across the models, assuming a Gaussian distribution. Vertical lines represent estimates from the  
machine learning-based dataset UpCH<sub>4</sub>, with different colors corresponding to different climate datasets. b. Time series of anomalies for  
370 2019 for GSWP3. The shaded area in  $\Delta\text{Fw}$  represents the minimum and maximum range from the prognostic model simulations. Dashed  
lines are linear fitted trends for corresponding variables.

### 3.4 Temperature sensitivity of wetland CH<sub>4</sub> models

The modeled CH<sub>4</sub> emissions show an exponential relationship between eCH<sub>4</sub> and air temperature, with higher temperatures  
375 corresponding to higher mean eCH<sub>4</sub> during the peak growing season (JJA, June-July-August) in the Northern Hemisphere (Fig.  
4a). The model ensemble mean of eCH<sub>4</sub> response to temperature shows good agreement within the range of the spread when  
compared to the site-level measurements from FLUXNET-CH<sub>4</sub> and the gridded product UpCH<sub>4</sub>. The model ensemble mean  
has a higher CH<sub>4</sub> emitting strength (i.e., CH<sub>4</sub> emission per standard wetland area) for the high latitudes, leading to lower  
apparent Q<sub>10</sub>. This implies that the model ensemble estimated temperature sensitivity for the high latitudes could be potentially  
380 overestimated during the JJA season. The apparent Q<sub>10</sub> values for individual models show a large spread (Fig. S9), with eleven  
out of the sixteen models having statistically significant ( $p < 0.01$ ) exponential relationships. The good agreement between the  
ensemble mean and observations suggest that the ensemble approach provides a better constraint compared to single models  
alone. Furthermore, it is important to acknowledge that the sparse spatial coverage of FLUXNET-CH<sub>4</sub> over low latitudes,  
especially for underrepresented areas such as Africa, Southeast Asia, and South America, limits our ability to evaluate  
385 temperature dependencies over high-temperature regions (Fig. S10).

The modeled apparent Q<sub>10</sub> exhibits an average temperature dependence similar to that of ecosystem respiration, as reported by  
previous studies (Bloom et al., 2017; Mahecha et al., 2010; Yvon-Durocher et al., 2014), indicating that the underlying factors  
controlling the response of eCH<sub>4</sub> and ecosystem respiration to temperature covary. The modeled temperature dependences are  
390 more constrained with less spread for JJA and SON (September-October-November) than DJF (December-January-February)  
and MAM (March-April-May) when most site-level measurements have limited availability. The seasonal variations of  
modeled apparent Q<sub>10</sub> differ from site-level observations or UpCH<sub>4</sub>, reflecting discrepancies in the involved processes between  
eddy covariance and land surface models. Given that underrepresented processes such as substrate supply tend to have higher  
sensitivity of ecosystem metabolic processes to temperature, it is likely that the models do not entirely capture the fine-scale  
395 processes that affect the overall temperature response (Chang et al. 2021). In addition, the absence or underrepresentation of  
certain biophysical processes could lead to lower modeled apparent Q<sub>10</sub>. For instance, the ensemble mean of modeled apparent

Q<sub>10</sub> for SON seasons is underestimated, likely linked to the limited representation of processes during the freeze/thaw cycle (e.g., zero-curtain period), as suggested by previous observational studies (Mastepanov et al., 2008; Zona et al., 2016).



400

**Figure 4. Temperature sensitivity of simulated seasonal eCH<sub>4</sub> across locations of FLUXNET-CH<sub>4</sub> sites.** a. Model ensemble mean (‘Model Ensmean’) of simulated eCH<sub>4</sub> against seasonal mean temperature for the JJA season along the temperature gradient at the locations of FLUXNET-CH<sub>4</sub> sites in comparison to the estimates from eddy covariance measurements (‘Obs’; Fig. S10; Table S4) and UpCH<sub>4</sub>. Each dot represents the value at one site for an individual year when observations are available. The unit of the simulated CH<sub>4</sub> emissions is g CH<sub>4</sub> m<sup>-1</sup> month<sup>-1</sup> per standard wetland area to exclude the effect of inundation on eCH<sub>4</sub>. The exponential fitted curves are shown. b. Histogram of the seasonal Q<sub>10</sub> for the 16 individual models for the months DJF, MAM, JJA, and SON. Sample sizes are shown in the plot. The Q<sub>10</sub> values derived from FLUXNET-CH<sub>4</sub>, UpCH<sub>4</sub>, and the model ensemble mean are vertical solid lines, with a width of the bar for ‘Obs’ indicating the uncertainty range of Q<sub>10</sub> based on measurement uncertainty.

#### 410 4 Conclusions

Our results estimated global average wetland CH<sub>4</sub> emissions at  $158 \pm 24$  (mean  $\pm 1\sigma$ ) Tg CH<sub>4</sub> yr<sup>-1</sup> for the period 2010-2020, with an average decadal increase of 6-7 Tg CH<sub>4</sub> yr<sup>-1</sup> compared to the decade of 2000-2009. The increases in the four latitudinal

bands of 90°S-30°S, 30°S- 30°N, 30°N-60°N, and 60°N-90°N were 0.1-0.2 Tg CH<sub>4</sub> yr<sup>-1</sup>, 3.6-3.7 Tg CH<sub>4</sub> yr<sup>-1</sup>, 1.8-2.4 Tg CH<sub>4</sub> yr<sup>-1</sup>, and 0.6-0.8 Tg CH<sub>4</sub> yr<sup>-1</sup>, respectively, during the two decades. Our analysis reveals how global wetlands respond to variations in the primary climatic controls of temperature, precipitation, and rising CO<sub>2</sub> concentrations. The model average shows good agreement with eddy covariance measurements on temperature dependence, confirming the primary role of temperature in the rising trajectory of eCH<sub>4</sub> at decadal timescales. Furthermore, the modeled ensembles of prognostic wetland extents offer a complementary approach to satellite-based estimates (Prigent et al., 2020; Zhang, et al., 2021a) and enable further investigation into the uncertainties in wetland area estimation. These differences can motivate improvements to inundation schemes through an improved water table position (Chen et al., 2021) and lateral flow representation. Note that a large portion of tropical wetlands comprises inundated floodplains connecting rivers, where the leaching of methane production from wetlands to river networks is not accounted for in the wetland models. The prognostic models estimate an annual mean maximum wetland area of 8.0±2.0 Mkm<sup>2</sup>, with a seasonal cycle (annual maximum minus annual minimum) of 4.7±2.0 Mkm<sup>2</sup>. Resolving the large uncertainty in wetland areas and seasonal variation remains a high priority to refine bottom-up estimates of eCH<sub>4</sub>. Lastly, our results highlight the important but highly uncertain CO<sub>2</sub> fertilization effect on eCH<sub>4</sub>. The mean sensitivity coefficient  $\beta$  and results from the factorial experiment suggest a net increase of eCH<sub>4</sub> of 0.1%-2.3% relative to the annual total under an average ~20 ppm increase in atmospheric CO<sub>2</sub> concentration. In comparison, a synthesis study based on field experiments (van Groenigen et al., 2011) shows a narrower range of 0.3%-0.6% average increase for every 20 ppm increase, assuming a linear fertilization effect between CO<sub>2</sub> concentration and eCH<sub>4</sub>.

430

Our results show that an ensemble of process-based wetland methane models provides quantification for uncertainty in eCH<sub>4</sub>, as well as better constraints than a single model on the predicted trend and magnitude of eCH<sub>4</sub>. However, nominally distinct models might have similar biases because of similarities in the way they represent a subset of processes (see Table S1 for the model summary). Future evaluation of modeled processes, such as oxidation, production, and transport pathways, along with model error across different time scales using statistical tools could help identify similarities in model behaviors to guide model development (Zhang, 2023b). Furthermore, the eCH<sub>4</sub> estimates are subject to forcing uncertainty, given that the two climate datasets applied in the simulation protocol do not cover the full magnitude and variability of climatic variables. Specifically, precipitation has a significant impact on wetland extent and anaerobic soil conditions but has large uncertainty in spatiotemporal patterns (Sun et al., 2018). Thus, we recommend future ensemble simulations consider the uncertainty in climate variables among different datasets. In addition, the sensitivity parameters derived from the multiple regression are not independent of climate datasets. Thus, they are affected by the choice of meteorological drivers. Overall, quantitatively accounting for model performance and dependence and thoroughly evaluating the effectiveness (Chang et al., 2023) could improve the wetland model ensemble estimation in future studies.

445 **Code and data availability**



The code for the wetland models is available upon request from the respective model groups. The wetland ensemble results is publicly available at the Zenodo Repository 10.5281/zenodo.11309188. The wetland estimates from individual models are available upon request from respective model groups. The FLUXNET-CH<sub>4</sub> dataset is publicly available at the link: <https://fluxnet.org/data/fluxnet-ch4-community-product/>. The UpCH<sub>4</sub> dataset can be found at the link in McNicol et al., (2023).

450

### **Author contribution**

BP and ZZ designed the simulation experiment with contributions from JM and WR. ZZ conducted data collection and data analysis. JM, WR, GB, PC, NG, PH, AI, AJ, FJ, TK, TL, XL, PM, JM, CP, SP, ZQ, QS, HT, XX, YY, XY, WZ, QZ, QZ, QZ, and ZZ performed the simulations. ZZ prepared the manuscript with contributions from all co-authors.

### **Competing interests**

At least one of the (co-)authors is a member of the editorial board of Biogeosciences.

### **Acknowledgments**

This paper is the result of a collaborative international effort under the umbrella of the Global Carbon Project, a project of Future Earth, and a research partner of the World Climate Research Programme. Z.Z acknowledge support from National Natural Science Foundation of China Basic Science Center for Tibetan Plateau Earth System project. X. Y and S. Peng were funded by NSFC (41830643, 41722101). Thomas Kleinen acknowledges support from the German Federal Ministry of Education and Research (BMBF), Grant No. 01LP1921A. J.R.M. thanks Jade Skye for her assistance in running and processing the CLASSIC simulations. A. Ito was partly supported by MEXT Arcs-II. L. Liu and Q. Zhuang are supported by NASA project (NNX17AK20G). Q. Zhu and C. Peng are supported by the Second Tibetan Plateau Scientific Expedition (2019QZKK0304). J. Müller and F. Joos were supported by the Swiss National Science Foundation (#200020\_200511). Q. Zhu and W. Riley were supported by the Reducing Uncertainties in Biogeochemical Interactions through Synthesis and Computation (RUBISCO) Scientific Focus Area and Energy Exascale Earth System Modeling Project, which are sponsored by the Earth and Environmental Systems Modeling (EESM) Program under the Office of Biological and Environmental Research of the U.S. Department of Energy Office of Science. Y. Yao and H. Tian are funded in part by NSF program (award numbers: # 1903722) NASA CMS Program (award numbers: NX14AO73G). T. Li was supported by the National Key Scientific and Technological Infrastructure project “Earth System Science Numerical Simulator Facility” (EarthLab) and the Open Research Program of the International Research Center of Big Data for Sustainable Development Goals (Grant No. CBAS2023ORP02). P. Hopcroft was supported by a Birmingham Fellowship and the University of Birmingham's BlueBEAR HPC service. W.Z. acknowledges the support from the LUNARC computation project LU 2021/2-114 and the Swedish Research Council (Vetenskapsrådet) starting grant 2020-05338. W.Z. and P.A.M. acknowledge this study as a contribution to

the strategic research areas Modeling the Regional and Global Earth System (MERGE) and Biodiversity and Ecosystem  
480 Services in a Changing Climate (BECC) at Lund University. RB Jackson acknowledges support from the United Nations  
Environment Programme (UNEP) to Stanford University DTIE21-EN3143. N.G. was supported by the Newton Fund through  
the Met Office Climate Science for Service Partnership Brazil (CSSP Brazil). A. Jain and X. Xu were supported by the US  
National Science Foundation (NSF- 831361857) and would like to acknowledge the high-performance computing support  
485 from Cheyenne (doi:10.5065/D6RX-99HX) provided by NCAR's Computational and Information Systems Laboratory,  
sponsored by the National Science Foundation. P.C. acknowledges support from the space Agency Climate Change Initiative  
(ESA CCI) RECCAP2 project (grant no. ESRIN/4000123002/18/I-NB). JG Canadell acknowledges the support of the  
Australian National Environmental Climate Science Program - Climate Systems hub. G. McNicol acknowledges support from  
the NASA CMS program (award number: NNH20ZDA001N).

## 490 **References**

- Arndt, K. A., Oechel, W. C., Goodrich, J. P., Bailey, B. A., Kalhori, A., Hashemi, J., Sweeney, C., and Zona, D.: Sensitivity  
of Methane Emissions to Later Soil Freezing in Arctic Tundra Ecosystems, *Journal of Geophysical Research: Biogeosciences*,  
124, 2595–2609, <https://doi.org/10.1029/2019JG005242>, 2019.
- Arora, V. K., Melton, J. R., and Plummer, D.: An assessment of natural methane fluxes simulated by the CLASS-CTEM  
495 model, *Biogeosciences*, 15, 4683–4709, <https://doi.org/10.5194/bg-15-4683-2018>, 2018.
- Bansal, S., Post van der Burg, M., Fern, R. R., Jones, J. W., Lo, R., McKenna, O. P., Tangen, B. A., Zhang, Z., and Gleason,  
R. A.: Large increases in methane emissions expected from North America's largest wetland complex, *Science Advances*, 9,  
eade1112, <https://doi.org/10.1126/sciadv.ade1112>, 2023.
- Basso, L. S., Marani, L., Gatti, L. V., Miller, J. B., Gloor, M., Melack, J., Cassol, H. L. G., Tejada, G., Domingues, L. G., Arai,  
500 E., Sanchez, A. H., Corrêa, S. M., Anderson, L., Aragão, L. E. O. C., Correia, C. S. C., Crispim, S. P., and Neves, R. A. L.:  
Amazon methane budget derived from multi-year airborne observations highlights regional variations in emissions, *Commun  
Earth Environ*, 2, 1–13, <https://doi.org/10.1038/s43247-021-00314-4>, 2021.
- Bastviken, D., Treat, C. C., Pangala, S. R., Gauci, V., Enrich-Prast, A., Karlson, M., Gålfalk, M., Romano, M. B., and  
Sawakuchi, H. O.: The importance of plants for methane emission at the ecosystem scale, *Aquatic Botany*, 184, 103596,  
505 <https://doi.org/10.1016/j.aquabot.2022.103596>, 2023.
- Basu, S., Lan, X., Dlugokencky, E., Michel, S., Schwietzke, S., Miller, J. B., Bruhwiler, L., Oh, Y., Tans, P. P., Apadula, F.,  
Gatti, L. V., Jordan, A., Necki, J., Sasakawa, M., Morimoto, S., Di Iorio, T., Lee, H., Arduini, J., and Manca, G.: Estimating  
emissions of methane consistent with atmospheric measurements of methane and  $\delta^{13}\text{C}$  of methane, *Atmos. Chem. Phys.*, 22,

- 15351–15377, <https://doi.org/10.5194/acp-22-15351-2022>, 2022.
- 510 Bergamaschi, P., Houweling, S., Segers, A., Krol, M., Frankenberg, C., Scheepmaker, R. A., Dlugokencky, E., Wofsy, S. C., Kort, E. A., Sweeney, C., Schuck, T., Brenninkmeijer, C., Chen, H., Beck, V., and Gerbig, C.: Atmospheric CH<sub>4</sub> in the first decade of the 21st century: Inverse modeling analysis using SCIAMACHY satellite retrievals and NOAA surface measurements, *Journal of Geophysical Research: Atmospheres*, 118, 7350–7369, <https://doi.org/10.1002/jgrd.50480>, 2013.
- Bloom, A. A., Bowman, K. W., Lee, M., Turner, A. J., Schroeder, R., Worden, J. R., Weidner, R., McDonald, K. C., and  
515 Jacob, D. J.: A global wetland methane emissions and uncertainty dataset for atmospheric chemical transport models (WetCHARTs version 1.0), *Geoscientific Model Development*, 10, 2141–2156, <https://doi.org/10.5194/gmd-10-2141-2017>, 2017.
- Boening, C., Willis, J. K., Landerer, F. W., Nerem, R. S., and Fasullo, J.: The 2011 La Niña: So strong, the oceans fell: LA NIÑA 2011-SO STRONG, THE OCEANS FELL, *Geophysical Research Letters*, 39, n/a-n/a,  
520 <https://doi.org/10.1029/2012GL053055>, 2012.
- Bohn, T. J., Melton, J. R., Ito, A., Kleinen, T., Spahni, R., Stocker, B. D., Zhang, B., Zhu, X., Schroeder, R., Glagolev, M. V., Maksyutov, S., Brovkin, V., Chen, G., Denisov, S. N., Eliseev, A. V., Gallego-Sala, A., McDonald, K. C., Rawlins, M. A., Riley, W. J., Subin, Z. M., Tian, H., Zhuang, Q., and Kaplan, J. O.: WETCHIMP-WSL: intercomparison of wetland methane emissions models over West Siberia, *Biogeosciences*, 12, 3321–3349, <https://doi.org/10.5194/bg-12-3321-2015>, 2015.
- 525 [Bousquet, P., Ciais, P., Miller, J. B., Dlugokencky, E. J., Hauglustaine, D. A., Prigent, C., Van der Werf, G. R., Peylin, P., Brunke, E.-G., Carouge, C., Langenfelds, R. L., Lathière, J., Papa, F., Ramonet, M., Schmidt, M., Steele, L. P., Tyler, S. C., and White, J.: Contribution of anthropogenic and natural sources to atmospheric methane variability, \*Nature\*, 443, 439–443, <https://doi.org/10.1038/nature05132>, 2006.](https://doi.org/10.1038/nature05132)
- [Bridgman, S. D., Cadillo-Quiroz, H., Keller, J. K., and Zhuang, Q.: Methane emissions from wetlands: biogeochemical, microbial, and modeling perspectives from local to global scales, \*Global Change Biology\*, 19, 1325–1346, <https://doi.org/10.1111/gcb.12131>, 2013.](https://doi.org/10.1111/gcb.12131)
- 530 Cao, M., Marshall, S., and Gregson, K.: Global carbon exchange and methane emissions from natural wetlands: Application of a process-based model, *Journal of Geophysical Research: Atmospheres*, 101, 14399–14414, <https://doi.org/10.1029/96JD00219>, 1996.
- 535 Chang, K.-Y., Riley, W. J., Crill, P. M., Grant, R. F., and Saleska, S. R.: Hysteretic temperature sensitivity of wetland CH<sub>4</sub> fluxes explained by substrate availability and microbial activity, *Biogeosciences*, 17, 5849–5860, <https://doi.org/10.5194/bg-17-5849-2020>, 2020.
- Chang, K.-Y., Riley, W. J., Knox, S. H., Jackson, R. B., McNicol, G., Poulter, B., Aurela, M., Baldocchi, D., Bansal, S., Bohrer, G., Campbell, D. I., Cescatti, A., Chu, H., Delwiche, K. B., Desai, A. R., Euskirchen, E., Friborg, T., Goeckede, M.,

- 540 Helbig, M., Hemes, K. S., Hirano, T., Iwata, H., Kang, M., Keenan, T., Krauss, K. W., Lohila, A., Mammarella, I., Mitra, B., Miyata, A., Nilsson, M. B., Noormets, A., Oechel, W. C., Papale, D., Peichl, M., Reba, M. L., Rinne, J., Runkle, B. R. K., Ryu, Y., Sachs, T., Schäfer, K. V. R., Schmid, H. P., Shurpali, N., Sonnentag, O., Tang, A. C. I., Torn, M. S., Trotta, C., Tuittila, E.-S., Ueyama, M., Vargas, R., Vesala, T., Windham-Myers, L., Zhang, Z., and Zona, D.: Substantial hysteresis in emergent temperature sensitivity of global wetland CH<sub>4</sub> emissions, *Nature Communications*, 12, 2266, <https://doi.org/10.1038/s41467-021-22452-1>, 2021.
- 545 Chang, K.-Y., Riley, W. J., Collier, N., McNicol, G., Fluet-Chouinard, E., Knox, S. H., Delwiche, K. B., Jackson, R. B., Poulter, B., Saunio, M., Chandra, N., Gedney, N., Ishizawa, M., Ito, A., Joos, F., Kleinen, T., Maggi, F., McNorton, J., Melton, J. R., Miller, P., Niwa, Y., Pasut, C., Patra, P. K., Peng, C., Peng, S., Segers, A., Tian, H., Tsuruta, A., Yao, Y., Yin, Y., Zhang, W., Zhang, Z., Zhu, Q., and Zhuang, Q.: Observational constraints reduce model spread but not uncertainty in global wetland methane emission estimates, *Global Change Biology*, 29, 4298–4312, <https://doi.org/10.1111/gcb.16755>, 2023.
- 550 Chang, R. Y.-W., Miller, C. E., Dinardo, S. J., Karion, A., Sweeney, C., Daube, B. C., Henderson, J. M., Mountain, M. E., Eluszkiewicz, J., Miller, J. B., Bruhwiler, L. M. P., and Wofsy, S. C.: Methane emissions from Alaska in 2012 from CARVE airborne observations, *Proceedings of the National Academy of Sciences*, 111, 16694–16699, <https://doi.org/10.1073/pnas.1412953111>, 2014.
- 555 Chu, H., Luo, X., Ouyang, Z., Chan, W. S., Dengel, S., Biraud, S. C., Torn, M. S., Metzger, S., Kumar, J., Arain, M. A., Arkebauer, T. J., Baldocchi, D., Bernacchi, C., Billesbach, D., Black, T. A., Blanken, P. D., Bohrer, G., Bracho, R., Brown, S., Brunsell, N. A., Chen, J., Chen, X., Clark, K., Desai, A. R., Duman, T., Durden, D., Fares, S., Forbrich, I., Gamon, J. A., Gough, C. M., Griffis, T., Helbig, M., Hollinger, D., Humphreys, E., Ikawa, H., Iwata, H., Ju, Y., Knowles, J. F., Knox, S. H., Kobayashi, H., Kolb, T., Law, B., Lee, X., Litvak, M., Liu, H., Munger, J. W., Noormets, A., Novick, K., Oberbauer, S. F.,
- 560 Oechel, W., Oikawa, P., Papuga, S. A., Pendall, E., Prajapati, P., Prueger, J., Quinton, W. L., Richardson, A. D., Russell, E. S., Scott, R. L., Starr, G., Staebler, R., Stoy, P. C., Stuart-Haëntjens, E., Sonnentag, O., Sullivan, R. C., Suyker, A., Ueyama, M., Vargas, R., Wood, J. D., and Zona, D.: Representativeness of Eddy-Covariance flux footprints for areas surrounding AmeriFlux sites, *Agricultural and Forest Meteorology*, 301–302, 108350, <https://doi.org/10.1016/j.agrformet.2021.108350>, 2021.
- 565 Cucchi, M., Weedon, G. P., Amici, A., Bellouin, N., Lange, S., Müller Schmied, H., Hersbach, H., and Buontempo, C.: WFDE5: bias-adjusted ERA5 reanalysis data for impact studies, *Earth System Science Data*, 12, 2097–2120, <https://doi.org/10.5194/essd-12-2097-2020>, 2020.
- 570 Delwiche, K. B., Knox, S. H., Malhotra, A., Fluet-Chouinard, E., McNicol, G., Feron, S., Ouyang, Z., Papale, D., Trotta, C., Canfora, E., Cheah, Y.-W., Christianson, D., Alberto, M. C. R., Alekseychik, P., Aurela, M., Baldocchi, D., Bansal, S., Billesbach, D. P., Bohrer, G., Bracho, R., Buchmann, N., Campbell, D. I., Celis, G., Chen, J., Chen, W., Chu, H., Dalmagro, H. J., Dengel, S., Desai, A. R., Detto, M., Dolman, H., Eichelmann, E., Euskirchen, E., Famulari, D., Fuchs, K., Goeckede,

- M., Gogo, S., Gondwe, M. J., Goodrich, J. P., Gottschalk, P., Graham, S. L., Heimann, M., Helbig, M., Helfter, C., Hemes, K. S., Hirano, T., Hollinger, D., Hörtnagl, L., Iwata, H., Jacotot, A., Jurasinski, G., Kang, M., Kasak, K., King, J., Klatt, J., Koebsch, F., Krauss, K. W., Lai, D. Y. F., Lohila, A., Mammarella, I., Belelli Marchesini, L., Manca, G., Matthes, J. H.,  
575 Maximov, T., Merbold, L., Mitra, B., Morin, T. H., Nemitz, E., Nilsson, M. B., Niu, S., Oechel, W. C., Oikawa, P. Y., Ono, K., Peichl, M., Peltola, O., Reba, M. L., Richardson, A. D., Riley, W., Runkle, B. R. K., Ryu, Y., Sachs, T., Sakabe, A., Sanchez, C. R., Schuur, E. A., Schäfer, K. V. R., Sonnentag, O., Sparks, J. P., Stuart-Haëntjens, E., Sturtevant, C., Sullivan, R. C., Szutu, D. J., Thom, J. E., Torn, M. S., Tuittila, E.-S., Turner, J., Ueyama, M., Valach, A. C., Vargas, R., Varlagin, A., et al.: FLUXNET-CH<sub>4</sub>: a global, multi-ecosystem dataset and analysis of methane seasonality from freshwater wetlands, Earth  
580 System Science Data, 13, 3607–3689, <https://doi.org/10.5194/essd-13-3607-2021>, 2021.
- Dirmeyer, P. A., Gao, X., Zhao, M., Guo, Z., Oki, T., and Hanasaki, N.: GSWP-2: Multimodel Analysis and Implications for Our Perception of the Land Surface, Bulletin of the American Meteorological Society, 87, 1381–1398, <https://doi.org/10.1175/BAMS-87-10-1381>, 2006.
- Feng, L., Palmer, P. I., Zhu, S., Parker, R. J., and Liu, Y.: Tropical methane emissions explain large fraction of recent changes  
585 in global atmospheric methane growth rate, Nature Communications, 13, 1378, <https://doi.org/10.1038/s41467-022-28989-z>, 2022.
- Fleischmann, A. and P., Fabrice and Hamilton, Stephen K. and Fassoni-Andrade, Alice and Wongchuig, Sly and Espinoza, Jhan Carlo and Paiva, Rodrigo and Melack, John and Fluet-Chouinard, Etienne and Castello, Leandro and Almeida, Rafael and Bonnet, Marie Paule and Gripp Alves, Luna and Moreira, Daniel and Yamazaki, Dai and Revel, Menaka and Collischonn,  
590 Walter: Increased floodplain inundation in the Amazon since 1980, Environmental Research Letters, 2023.
- Fluet-Chouinard, E., Stocker, B. D., Zhang, Z., Malhotra, A., Melton, J. R., Poulter, B., Kaplan, J. O., Goldewijk, K. K., Siebert, S., Minayeva, T., Hugelius, G., Joosten, H., Barthelmes, A., Prigent, C., Aires, F., Hoyt, A. M., Davidson, N., Finlayson, C. M., Lehner, B., Jackson, R. B., and McIntyre, P. B.: Extensive global wetland loss over the past three centuries, Nature, 614, 281–286, <https://doi.org/10.1038/s41586-022-05572-6>, 2023.
- 595 France, J. L., Lunt, M. F., Andrade, M., Moreno, I., Ganesan, A. L., Lachlan-Cope, T., Fisher, R. E., Lowry, D., Parker, R. J., Nisbet, E. G., and Jones, A. E.: Very large fluxes of methane measured above Bolivian seasonal wetlands, Proceedings of the National Academy of Sciences, 119, e2206345119, <https://doi.org/10.1073/pnas.2206345119>, 2022.
- Gatti, L. V., Basso, L. S., Miller, J. B., Gloor, M., Gatti Domingues, L., Cassol, H. L. G., Tejada, G., Aragão, L. E. O. C., Nobre, C., Peters, W., Marani, L., Arai, E., Sanches, A. H., Corrêa, S. M., Anderson, L., Von Randow, C., Correia, C. S. C.,  
600 Crispim, S. P., and Neves, R. A. L.: Amazonia as a carbon source linked to deforestation and climate change, Nature, 595, 388–393, <https://doi.org/10.1038/s41586-021-03629-6>, 2021.
- Gedney, N.: Climate feedback from wetland methane emissions, Geophysical Research Letters, 31, L20503,

<https://doi.org/10.1029/2004GL020919>, 2004.

Gerlein-Safdi, C., Bloom, A. A., Plant, G., Kort, E. A., and Ruf, C. S.: Improving Representation of Tropical Wetland Methane  
605 Emissions With CYGNSS Inundation Maps, *Global Biogeochemical Cycles*, 35, e2020GB006890,  
<https://doi.org/10.1029/2020GB006890>, 2021.

Glagolev, M., Kleptsova, I., Filippov, I., Maksyutov, S., and Machida, T.: Regional methane emission from West Siberia mire  
landscapes, *Environmental Research Letters*, 6, 045214, <https://doi.org/10.1088/1748-9326/6/4/045214>, 2011.

Gloor, M., Gatti, L. V., Wilson, C., Parker, R. J., Boesch, H., Popa, E., Chipperfield, M. P., Poulter, B., Zhang, Z., Basso, L.,  
610 Miller, J., McNorton, J., Jimenez, C., and Prigent, C.: Large Methane Emissions From the Pantanal During Rising Water-  
Levels Revealed by Regularly Measured Lower Troposphere CH<sub>4</sub> Profiles, *Global Biogeochemical Cycles*, 35,  
e2021GB006964, <https://doi.org/10.1029/2021GB006964>, 2021.

Grant, R. F., Mekonnen, Z. A., Riley, W. J., Arora, B., and Torn, M. S.: Mathematical Modelling of Arctic Polygonal Tundra  
with Ecosys: 2. Microtopography Determines How CO<sub>2</sub> and CH<sub>4</sub> Exchange Responds to Changes in Temperature and  
615 Precipitation, *Journal of Geophysical Research: Biogeosciences*, 122, 3174–3187, <https://doi.org/10.1002/2017JG004037>,  
2017.

Harris, I., Jones, P. D., Osborn, T. J., and Lister, D. H.: Updated high-resolution grids of monthly climatic observations - the  
CRU TS3.10 Dataset: UPDATED HIGH-RESOLUTION GRIDS OF MONTHLY CLIMATIC OBSERVATIONS,  
*International Journal of Climatology*, 34, 623–642, <https://doi.org/10.1002/joc.3711>, 2014.

620 Hopcroft, P. O., Valdes, P. J., O'Connor, F. M., Kaplan, J. O., and Beerling, D. J.: Understanding the glacial methane cycle,  
*Nature Communications*, 8, 14383, <https://doi.org/10.1038/ncomms14383>, 2017.

Kaiser, S., Göckede, M., Castro-Morales, K., Knoblauch, C., Ekici, A., Kleinen, T., Zubrzycki, S., Sachs, T., Wille, C., and  
Beer, C.: Process-based modelling of the methane balance in periglacial landscapes (JSBACH-methane), *Geoscientific Model  
Development*, 10, 333–358, <https://doi.org/10.5194/gmd-10-333-2017>, 2017.

625 Kirschke, S., Bousquet, P., Ciais, P., Saunoy, M., Canadell, J. G., Dlugokencky, E. J., Bergamaschi, P., Bergmann, D., Blake,  
D. R., Bruhwiler, L., Cameron-Smith, P., Castaldi, S., Chevallier, F., Feng, L., Fraser, A., Heimann, M., Hodson, E. L.,  
Houweling, S., Josse, B., Fraser, P. J., Krummel, P. B., Lamarque, J.-F., Langenfelds, R. L., Le Quéré, C., Naik, V., O'Doherty,  
S., Palmer, P. I., Pison, I., Plummer, D., Poulter, B., Prinn, R. G., Rigby, M., Ringeval, B., Santini, M., Schmidt, M., Shindell,  
D. T., Simpson, I. J., Spahni, R., Steele, L. P., Strode, S. A., Sudo, K., Szopa, S., van der Werf, G. R., Voulgarakis, A., van  
630 Weele, M., Weiss, R. F., Williams, J. E., and Zeng, G.: Three decades of global methane sources and sinks, *Nature Geoscience*,  
6, 813–823, <https://doi.org/10.1038/ngeo1955>, 2013.

Kleinen, T., Gromov, S., Steil, B., and Brovkin, V.: Atmospheric methane since the last glacial maximum was driven by  
wetland sources, *Clim. Past*, 19, 1081–1099, <https://doi.org/10.5194/cp-19-1081-2023>, 2023.

- 635 Knox, S. H., Jackson, R. B., Poulter, B., McNicol, G., Fluet-Chouinard, E., Zhang, Z., Hugelius, G., Bousquet, P., Canadell, J. G., Saunois, M., Papale, D., Chu, H., Keenan, T. F., Baldocchi, D., Torn, M. S., Mammarella, I., Trotta, C., Aurela, M., Bohrer, G., Campbell, D. I., Cescatti, A., Chamberlain, S., Chen, J., Chen, W., Dengel, S., Desai, A. R., Euskirchen, E., Friborg, T., Gasbarra, D., Goded, I., Goeckede, M., Heimann, M., Helbig, M., Hirano, T., Hollinger, D. Y., Iwata, H., Kang, M., Klatt, J., Krauss, K. W., Kutzbach, L., Lohila, A., Mitra, B., Morin, T. H., Nilsson, M. B., Niu, S., Noormets, A., Oechel, W. C., Peichl, M., Peltola, O., Reba, M. L., Richardson, A. D., Runkle, B. R. K., Ryu, Y., Sachs, T., Schäfer, K. V. R., Schmid, H.,
- 640 P., Shurpali, N., Sonnentag, O., Tang, A. C. I., Ueyama, M., Vargas, R., Vesala, T., Ward, E. J., Windham-Myers, L., Wohlfahrt, G., and Zona, D.: FLUXNET-CH<sub>4</sub> Synthesis Activity: Objectives, Observations, and Future Directions, *Bull. Amer. Meteor. Soc.*, 100, 2607–2632, <https://doi.org/10.1175/BAMS-D-18-0268.1>, 2019.
- Koffi, E. N., Bergamaschi, P., Alkama, R., and Cescatti, A.: An observation-constrained assessment of the climate sensitivity and future trajectories of wetland methane emissions, *Science Advances*, 6, eaay4444, <https://doi.org/10.1126/sciadv.aay4444>,
- 645 2020.
- Kuhn, M. A., Varner, R. K., Bastviken, D., Crill, P., MacIntyre, S., Turetsky, M., Walter Anthony, K., McGuire, A. D., and Olefeldt, D.: BAWLD-CH<sub>4</sub>: a comprehensive dataset of methane fluxes from boreal and arctic ecosystems, *Earth System Science Data*, 13, 5151–5189, <https://doi.org/10.5194/essd-13-5151-2021>, 2021.
- Li, M., Kort, E. A., Bloom, A. A., Wu, D., Plant, G., Gerlein-Safdi, C., and Pu, T.: Underestimated Dry Season Methane
- 650 Emissions from Wetlands in the Pantanal, *Environ. Sci. Technol.*, 58, 3278–3287, <https://doi.org/10.1021/acs.est.3c09250>, 2024.
- Lan, X., Basu, S., Schwietzke, S., Bruhwiler, L. M. P., Dlugokencky, E. J., Michel, S. E., Sherwood, O. A., Tans, P. P., Thoning, K., Etiope, G., Zhuang, Q., Liu, L., Oh, Y., Miller, J. B., Pétron, G., Vaughn, B. H., and Crippa, M.: Improved Constraints on Global Methane Emissions and Sinks Using  $\delta^{13}\text{C-CH}_4$ , *Global Biogeochemical Cycles*, 35, e2021GB007000,
- 655 <https://doi.org/10.1029/2021GB007000>, 2021.
- Lunt, M. F., Palmer, P. I., Lorente, A., Borsdorff, T., Landgraf, J., Parker, R. J., and Boesch, H.: Rain-fed pulses of methane from East Africa during 2018–2019 contributed to atmospheric growth rate, *Environmental Research Letters*, 16, 024021, <https://doi.org/10.1088/1748-9326/abd8fa>, 2021.
- Mahecha, M. D., Reichstein, M., Carvalhais, N., Lasslop, G., Lange, H., Seneviratne, S. I., Vargas, R., Ammann, C., Arain,
- 660 M. A., Cescatti, A., Janssens, I. A., Migliavacca, M., Montagnani, L., and Richardson, A. D.: Global Convergence in the Temperature Sensitivity of Respiration at Ecosystem Level, *Science*, 329, 838–840, <https://doi.org/10.1126/science.1189587>, 2010.
- Mastepanov, M., Sigsgaard, C., Dlugokencky, E. J., Houweling, S., Ström, L., Tamstorf, M. P., and Christensen, T. R.: Large tundra methane burst during onset of freezing, *Nature*, 456, 628–630, <https://doi.org/10.1038/nature07464>, 2008.



- 665 McNicol, G., Fluet-Chouinard, E., Ouyang, Z., Knox, S., Zhang, Z., Aalto, T., Bansal, S., Chang, K.-Y., Chen, M., Delwiche, K., Feron, S., Goeckede, M., Liu, J., Malhotra, A., Melton, J. R., Riley, W., Vargas, R., Yuan, K., Ying, Q., Zhu, Q., Alekseychik, P., Aurela, M., Billesbach, D. P., Campbell, D. I., Chen, J., Chu, H., Desai, A. R., Euskirchen, E., Goodrich, J., Griffis, T., Helbig, M., Hirano, T., Iwata, H., Jurasinski, G., King, J., Koebisch, F., Kolka, R., Krauss, K., Lohila, A., Mammarella, I., Nilson, M., Noormets, A., Oechel, W., Peichl, M., Sachs, T., Sakabe, A., Schulze, C., Sonntag, O., Sullivan,
- 670 R. C., Tuittila, E.-S., Ueyama, M., Vesala, T., Ward, E., Wille, C., Wong, G. X., Zona, D., Windham-Myers, L., Poulter, B., and Jackson, R. B.: Upscaling Wetland Methane Emissions From the FLUXNET-CH4 Eddy Covariance Network (UpCH4 v1.0): Model Development, Network Assessment, and Budget Comparison, *AGU Advances*, 4, e2023AV000956, <https://doi.org/10.1029/2023AV000956>, 2023.
- Meinshausen, M., Vogel, E., Nauels, A., Lorbacher, K., Meinshausen, N., Etheridge, D. M., Fraser, P. J., Montzka, S. A.,
- 675 Rayner, P. J., Trudinger, C. M., Krummel, P. B., Beyerle, U., Canadell, J. G., Daniel, J. S., Enting, I. G., Law, R. M., Lunder, C. R., O'Doherty, S., Prinn, R. G., Reimann, S., Rubino, M., Velders, G. J. M., Vollmer, M. K., Wang, R. H. J., and Weiss, R.: Historical greenhouse gas concentrations for climate modelling (CMIP6), *Geoscientific Model Development*, 10, 2057–2116, <https://doi.org/10.5194/gmd-10-2057-2017>, 2017.
- Melton, J. R., Wania, R., Hodson, E. L., Poulter, B., Ringeval, B., Spahni, R., Bohn, T., Avis, C. A., Beerling, D. J., Chen, G.,
- 680 Eliseev, A. V., Denisov, S. N., Hopcroft, P. O., Lettenmaier, D. P., Riley, W. J., Singarayer, J. S., Subin, Z. M., Tian, H., Zürcher, S., Brovkin, V., van Bodegom, P. M., Kleinen, T., Yu, Z. C., and Kaplan, J. O.: Present state of global wetland extent and wetland methane modelling: conclusions from a model inter-comparison project (WETCHIMP), *Biogeosciences*, 10, 753–788, <https://doi.org/10.5194/bg-10-753-2013>, 2013.
- Miller, S. M., Miller, C. E., Commane, R., Chang, R. Y.-W., Dinardo, S. J., Henderson, J. M., Karion, A., Lindaas, J., Melton,
- 685 J. R., Miller, J. B., Sweeney, C., Wofsy, S. C., and Michalak, A. M.: A multiyear estimate of methane fluxes in Alaska from CARVE atmospheric observations: METHANE FLUXES FROM ALASKA, *Global Biogeochemical Cycles*, 30, 1441–1453, <https://doi.org/10.1002/2016GB005419>, 2016.
- Natali, S. M., Watts, J. D., Rogers, B. M., Potter, S., Ludwig, S. M., Selbmann, A.-K., Sullivan, P. F., Abbott, B. W., Arndt,
- K. A., Birch, L., Björkman, M. P., Bloom, A. A., Celis, G., Christensen, T. R., Christiansen, C. T., Commane, R., Cooper, E.
- 690 J., Crill, P., Czimczik, C., Davydov, S., Du, J., Egan, J. E., Elberling, B., Euskirchen, E. S., Friborg, T., Genet, H., Goeckede, M., Goodrich, J. P., Grogan, P., Helbig, M., Jafarov, E. E., Jastrow, J. D., Kalhori, A. A. M., Kim, Y., Kimball, J. S., Kutzbach, L., Lara, M. J., Larsen, K. S., Lee, B.-Y., Liu, Z., Loranty, M. M., Lund, M., Lupascu, M., Madani, N., Malhotra, A., Matamala, R., McFarland, J., McGuire, A. D., Michelsen, A., Minions, C., Oechel, W. C., Olefeldt, D., Parmentier, F.-J. W., Pirk, N., Poulter, B., Quinton, W., Rezanezhad, F., Risk, D., Sachs, T., Schaefer, K., Schmidt, N. M., Schuur, E. A. G., Semenchuk, P.
- 695 R., Shaver, G., Sonntag, O., Starr, G., Treat, C. C., Waldrop, M. P., Wang, Y., Welker, J., Wille, C., Xu, X., Zhang, Z., Zhuang, Q., and Zona, D.: Large loss of CO<sub>2</sub> in winter observed across the northern permafrost region, *Nature Climate Change*,



- 9, 852–857, <https://doi.org/10.1038/s41558-019-0592-8>, 2019.
- Nisbet, E. G., Manning, M. R., Dlugokencky, E. J., Fisher, R. E., Lowry, D., Michel, S. E., Myhre, C. L., Platt, S. M., Allen, G., Bousquet, P., Brownlow, R., Cain, M., France, J. L., Hermansen, O., Hossaini, R., Jones, A. E., Levin, I., Manning, A. C.,  
700 Myhre, G., Pyle, J. A., Vaughn, B. H., Warwick, N. J., and White, J. W. C.: Very Strong Atmospheric Methane Growth in the 4 Years 2014–2017: Implications for the Paris Agreement, *Global Biogeochemical Cycles*, 2018GB006009, <https://doi.org/10.1029/2018GB006009>, 2019.
- Nisbet, E. G., Manning, M. R., Dlugokencky, E. J., Michel, S. E., Lan, X., Röckmann, T., Denier van der Gon, H. A. C., Schmitt, J., Palmer, P. I., Dyonisius, M. N., Oh, Y., Fisher, R. E., Lowry, D., France, J. L., White, J. W. C., Brailsford, G., and  
705 Bromley, T.: Atmospheric Methane: Comparison Between Methane’s Record in 2006–2022 and During Glacial Terminations, *Global Biogeochemical Cycles*, 37, e2023GB007875, <https://doi.org/10.1029/2023GB007875>, 2023.
- Palmer, P. I., Woodwark, A. J. P., Finch, D. P., Taylor, T. E., Butz, A., Tamminen, J., Bösch, H., Eldering, A., and Vincent-Bonnieu, S.: Role of space station instruments for improving tropical carbon flux estimates using atmospheric data, *npj Microgravity*, 8, 51, <https://doi.org/10.1038/s41526-022-00231-6>, 2022.
- 710 Pandey, S., Houweling, S., Lorente, A., Borsdorff, T., Tsvilidou, M., Bloom, A. A., Poulter, B., Zhang, Z., and Aben, I.: Using satellite data to identify the methane emission controls of South Sudan’s wetlands, *Biogeosciences*, 18, 557–572, <https://doi.org/10.5194/bg-18-557-2021>, 2021.
- Parker, R. J., Wilson, C., Bloom, A. A., Comyn-Platt, E., Hayman, G., McNorton, J., Boesch, H., and Chipperfield, M. P.: Exploring constraints on a wetland methane emission ensemble (WetCHARTs) using GOSAT observations, *Biogeosciences*,  
715 17, 5669–5691, <https://doi.org/10.5194/bg-17-5669-2020>, 2020.
- Patra, P. K., Houweling, S., Krol, M., Bousquet, P., Belikov, D., Bergmann, D., Bian, H., Cameron-Smith, P., Chipperfield, M. P., Corbin, K., Fortems-Cheiney, A., Fraser, A., Gloor, E., Hess, P., Ito, A., Kawa, S. R., Law, R. M., Loh, Z., Maksyutov, S., Meng, L., Palmer, P. I., Prinn, R. G., Rigby, M., Saito, R., and Wilson, C.: TransCom model simulations of CH<sub>4</sub> and related species: linking transport, surface flux and chemical loss with CH<sub>4</sub> variability in the troposphere and lower stratosphere,  
720 *Atmospheric Chemistry and Physics*, 11, 12813–12837, <https://doi.org/10.5194/acp-11-12813-2011>, 2011.
- Peng, S., Lin, X., Thompson, R. L., Xi, Y., Liu, G., Hauglustaine, D., Lan, X., Poulter, B., Ramonet, M., Saunois, M., Yin, Y., Zhang, Z., Zheng, B., and Ciais, P.: Wetland emission and atmospheric sink changes explain methane growth in 2020, *Nature*, 612, 477–482, <https://doi.org/10.1038/s41586-022-05447-w>, 2022.
- Petrescu, A. M. R., van Beek, L. P. H., van Huissteden, J., Prigent, C., Sachs, T., Corradi, C. A. R., Parmentier, F. J. W., and  
725 Dolman, A. J.: Modeling regional to global CH<sub>4</sub> emissions of boreal and arctic wetlands: Modeling Global CH<sub>4</sub> Emissions, *Global Biogeochemical Cycles*, 24, <https://doi.org/10.1029/2009GB003610>, 2010.
- Piao, S., Sitch, S., Ciais, P., Friedlingstein, P., Peylin, P., Wang, X., Ahlström, A., Anav, A., Canadell, J. G., Cong, N.,

- Huntingford, C., Jung, M., Levis, S., Levy, P. E., Li, J., Lin, X., Lomas, M. R., Lu, M., Luo, Y., Ma, Y., Myneni, R. B., Poulter, B., Sun, Z., Wang, T., Viovy, N., Zachle, S., and Zeng, N.: Evaluation of terrestrial carbon cycle models for their response to climate variability and to CO<sub>2</sub> trends, *Global Change Biology*, 19, 2117–2132, <https://doi.org/10.1111/gcb.12187>, 2013.
- Pickett-Heaps, C. A., Jacob, D. J., Wecht, K. J., Kort, E. A., Wofsy, S. C., Diskin, G. S., Worthy, D. E. J., Kaplan, J. O., Bey, I., and Drevet, J.: Magnitude and seasonality of wetland methane emissions from the Hudson Bay Lowlands (Canada), *Atmospheric Chemistry and Physics*, 11, 3773–3779, <https://doi.org/10.5194/acp-11-3773-2011>, 2011.
- 735 Poulter, B., Bousquet, P., Canadell, J. G., Ciais, P., Peregon, A., Saunio, M., Arora, V. K., Beerling, D. J., Brovkin, V., Jones, C. D., Joos, F., Gedney, N., Ito, A., Kleinen, T., Koven, C. D., McDonald, K., Melton, J. R., Peng, C., Peng, S., Prigent, C., Schroeder, R., Riley, W. J., Saito, M., Spahni, R., Tian, H., Taylor, L., Viovy, N., Wilton, D., Wiltshire, A., Xu, X., Zhang, B., Zhang, Z., and Zhu, Q.: Global wetland contribution to 2000–2012 atmospheric methane growth rate dynamics, *Environmental Research Letters*, 12, 094013, <https://doi.org/10.1088/1748-9326/aa8391>, 2017.
- 740 Prigent, C., Jimenez, C., and Bousquet, P.: Satellite-Derived Global Surface Water Extent and Dynamics Over the Last 25 Years (GIEMS-2), *Journal of Geophysical Research: Atmospheres*, 125, e2019JD030711, <https://doi.org/10.1029/2019JD030711>, 2020.
- Ringeval, B., Houweling, S., van Bodegom, P. M., Spahni, R., van Beek, R., Joos, F., and Röckmann, T.: Methane emissions from floodplains in the Amazon Basin: challenges in developing a process-based model for global applications, *Biogeosciences*, 11, 1519–1558, <https://doi.org/10.5194/bg-11-1519-2014>, 2014.
- Rößger, N., Sachs, T., Wille, C., Boike, J., and Kutzbach, L.: Seasonal increase of methane emissions linked to warming in Siberian tundra, *Nature Climate Change*, 12, 1031–1036, <https://doi.org/10.1038/s41558-022-01512-4>, 2022.
- Saunio, M., Bousquet, P., Poulter, B., Peregon, A., Ciais, P., Canadell, J. G., Dlugokencky, E. J., Etiope, G., Bastviken, D., Houweling, S., Janssens-Maenhout, G., Tubiello, F. N., Castaldi, S., Jackson, R. B., Alexe, M., Arora, V. K., Beerling, D. J., Bergamaschi, P., Blake, D. R., Brailsford, G., Brovkin, V., Bruhwiler, L., Crevoisier, C., Crill, P., Covey, K., Curry, C., Frankenberg, C., Gedney, N., Höglund-Isaksson, L., Ishizawa, M., Ito, A., Joos, F., Kim, H.-S., Kleinen, T., Krummel, P., Lamarque, J.-F., Langenfelds, R., Locatelli, R., Machida, T., Maksyutov, S., McDonald, K. C., Marshall, J., Melton, J. R., Morino, I., Naik, V., O’Doherty, S., Parmentier, F.-J. W., Patra, P. K., Peng, C., Peng, S., Peters, G. P., Pison, I., Prigent, C., Prinn, R., Ramonet, M., Riley, W. J., Saito, M., Santini, M., Schroeder, R., Simpson, I. J., Spahni, R., Steele, P., Takizawa, A., Thornton, B. F., Tian, H., Tohjima, Y., Viovy, N., Voulgarakis, A., van Weele, M., van der Werf, G. R., Weiss, R., Wiedinmyer, C., Wilton, D. J., Wiltshire, A., Worthy, D., Wunch, D., Xu, X., Yoshida, Y., Zhang, B., Zhang, Z., and Zhu, Q.: The Global Methane Budget 2000–2012, *Earth System Science Data*, 8, 697–751, <https://doi.org/10.5194/essd-8-697-2016>, 2016.

Saunois, M., Stavert, A. R., Poulter, B., Bousquet, P., Canadell, J. G., Jackson, R. B., Raymond, P. A., Dlugokencky, E. J.,  
760 Houweling, S., Patra, P. K., Ciais, P., Arora, V. K., Bastviken, D., Bergamaschi, P., Blake, D. R., Brailsford, G., Bruhwiler,  
L., Carlson, K. M., Carrol, M., Castaldi, S., Chandra, N., Crevoisier, C., Crill, P. M., Covey, K., Curry, C. L., Etiope, G.,  
Frankenberg, C., Gedney, N., Hegglin, M. I., Höglund-Isaksson, L., Hugelius, G., Ishizawa, M., Ito, A., Janssens-Maenhout,  
G., Jensen, K. M., Joos, F., Kleinen, T., Krummel, P. B., Langenfelds, R. L., Laruelle, G. G., Liu, L., Machida, T., Maksyutov,  
S., McDonald, K. C., McNorton, J., Miller, P. A., Melton, J. R., Morino, I., Müller, J., Murguia-Flores, F., Naik, V., Niwa, Y.,  
765 Noce, S., O'Doherty, S., Parker, R. J., Peng, C., Peng, S., Peters, G. P., Prigent, C., Prinn, R., Ramonet, M., Regnier, P., Riley,  
W. J., Rosentreter, J. A., Segers, A., Simpson, I. J., Shi, H., Smith, S. J., Steele, L. P., Thornton, B. F., Tian, H., Tohjima, Y.,  
Tubiello, F. N., Tsuruta, A., Viovy, N., Voulgarakis, A., Weber, T. S., van Weele, M., van der Werf, G. R., Weiss, R. F.,  
Worthy, D., Wunch, D., Yin, Y., Yoshida, Y., Zhang, W., Zhang, Z., Zhao, Y., Zheng, B., Zhu, Q., Zhu, Q., and Zhuang, Q.:  
The Global Methane Budget 2000–2017, *Earth System Science Data*, 12, 1561–1623, [https://doi.org/10.5194/essd-12-1561-](https://doi.org/10.5194/essd-12-1561-2020)  
770 [2020](https://doi.org/10.5194/essd-12-1561-2020), 2020.

Schaefer, K., Schwalm, C. R., Williams, C., Arain, M. A., Barr, A., Chen, J. M., Davis, K. J., Dimitrov, D., Hilton, T. W.,  
Hollinger, D. Y., Humphreys, E., Poulter, B., Raczka, B. M., Richardson, A. D., Sahoo, A., Thornton, P., Vargas, R., Verbeeck,  
H., Anderson, R., Baker, I., Black, T. A., Bolstad, P., Chen, J., Curtis, P. S., Desai, A. R., Dietze, M., Dragoni, D., Gough, C.,  
Grant, R. F., Gu, L., Jain, A., Kucharik, C., Law, B., Liu, S., Lokipitiya, E., Margolis, H. A., Matamala, R., McCaughey, J.  
775 H., Monson, R., Munger, J. W., Oechel, W., Peng, C., Price, D. T., Ricciuto, D., Riley, W. J., Roulet, N., Tian, H., Tonitto, C.,  
Torn, M., Weng, E., and Zhou, X.: A model-data comparison of gross primary productivity: Results from the North American  
Carbon Program site synthesis, *Journal of Geophysical Research: Biogeosciences*, 117,  
<https://doi.org/10.1029/2012JG001960>, 2012.

Schaefer, H., Fletcher, S. E. M., Veidt, C., Lassey, K. R., Brailsford, G. W., Bromley, T. M., Dlugokencky, E. J., Michel, S.  
780 E., Miller, J. B., Levin, I., Lowe, D. C., Martin, R. J., Vaughn, B. H., and White, J. W. C.: A 21st-century shift from fossil-  
fuel to biogenic methane emissions indicated by  $^{13}\text{CH}_4$ , *Science*, 352, 80–84, <https://doi.org/10.1126/science.aad2705>, 2016.

Shaw, J. T., Allen, G., Barker, P., Pitt, J. R., Pasternak, D., Bauguitte, S. J.-B., Lee, J., Bower, K. N., Daly, M. C., Lunt, M.  
F., Ganesan, A. L., Vaughan, A. R., Chibesakunda, F., Lambakasa, M., Fisher, R. E., France, J. L., Lowry, D., Palmer, P. I.,  
Metzger, S., Parker, R. J., Gedney, N., Bateson, P., Cain, M., Lorente, A., Borsdorff, T., and Nisbet, E. G.: Large Methane  
785 Emission Fluxes Observed From Tropical Wetlands in Zambia, *Global Biogeochemical Cycles*, 36, e2021GB007261,  
<https://doi.org/10.1029/2021GB007261>, 2022.

Shindell, D. and Smith, C. J.: Climate and air-quality benefits of a realistic phase-out of fossil fuels, *Nature*, 573, 408–411,  
<https://doi.org/10.1038/s41586-019-1554-z>, 2019.

Shu, S., Jain, A. K., and Kheshgi, H. S.: Investigating Wetland and Nonwetland Soil Methane Emissions and Sinks Across the  
790 Contiguous United States Using a Land Surface Model, *Global Biogeochemical Cycles*, 34, e2019GB006251,

- <https://doi.org/10.1029/2019GB006251>, 2020.
- Spahni, R., Wania, R., Neef, L., van Weele, M., Pison, I., Bousquet, P., Frankenberg, C., Foster, P. N., Joos, F., Prentice, I. C., and van Velthoven, P.: Constraining global methane emissions and uptake by ecosystems, *Biogeosciences*, 8, 1643–1665, <https://doi.org/10.5194/bg-8-1643-2011>, 2011.
- 795 Sun, Q., Miao, C., Duan, Q., Ashouri, H., Sorooshian, S., and Hsu, K.-L.: A Review of Global Precipitation Data Sets: Data Sources, Estimation, and Intercomparisons, *Reviews of Geophysics*, 56, 79–107, <https://doi.org/10.1002/2017RG000574>, 2018.
- Treat, C. C., Bloom, A. A., and Marushchak, M. E.: Nongrowing season methane emissions—a significant component of annual emissions across northern ecosystems, *Global Change Biology*, 24, 3331–3343, <https://doi.org/10.1111/gcb.14137>, 2018.
- 800 Tunnicliffe, R. L., Ganesan, A. L., Parker, R. J., Boesch, H., Gedney, N., Poulter, B., Zhang, Z., Lavrič, J. V., Walter, D., Rigby, M., Henne, S., Young, D., and O’Doherty, S.: Quantifying sources of Brazil’s CH<sub>4</sub> emissions between 2010 and 2018 from satellite data, *Atmospheric Chemistry and Physics Discussions*, 1–40, <https://doi.org/10.5194/acp-2020-438>, 2020.
- van Groenigen, K. J., Osenberg, C. W., and Hungate, B. A.: Increased soil emissions of potent greenhouse gases under increased atmospheric CO<sub>2</sub>, *Nature*, 475, 214–216, <https://doi.org/10.1038/nature10176>, 2011.
- 805 Wania, R., Melton, J. R., Hodson, E. L., Poulter, B., Ringeval, B., Spahni, R., Bohn, T., Avis, C. A., Chen, G., Eliseev, A. V., Hopcroft, P. O., Riley, W. J., Subin, Z. M., Tian, H., van Bodegom, P. M., Kleinen, T., Yu, Z. C., Singarayer, J. S., Zürcher, S., Lettenmaier, D. P., Beerling, D. J., Denisov, S. N., Prigent, C., Papa, F., and Kaplan, J. O.: Present state of global wetland extent and wetland methane modelling: methodology of a model inter-comparison project (WETCHIMP), *Geoscientific Model Development*, 6, 617–641, <https://doi.org/10.5194/gmd-6-617-2013>, 2013.
- 810 Wilson, C., Chipperfield, M. P., Gloor, M., Parker, R. J., Boesch, H., McNorton, J., Gatti, L. V., Miller, J. B., Basso, L. S., and Monks, S. A.: Large and increasing methane emissions from eastern Amazonia derived from satellite data, 2010–2018, *Atmospheric Chemistry and Physics*, 21, 10643–10669, <https://doi.org/10.5194/acp-21-10643-2021>, 2021.
- Wilson, C., Gloor, M., Gatti, L. V., Miller, J. B., Monks, S. A., McNorton, J., Bloom, A. A., Basso, L. S., and Chipperfield, M. P.: Contribution of regional sources to atmospheric methane over the Amazon Basin in 2010 and 2011: REGIONAL CH<sub>4</sub> SOURCES IN THE AMAZON BASIN, *Global Biogeochemical Cycles*, 30, 400–420, <https://doi.org/10.1002/2015GB005300>, 2016.
- Xi, Y., Peng, S., Ducharme, A., Ciais, P., Gumbrecht, T., Jimenez, C., Poulter, B., Prigent, C., Qiu, C., Saunois, M., and Zhang, Z.: Gridded maps of wetlands dynamics over mid-low latitudes for 1980–2020 based on TOPMODEL, *Scientific Data*, 9, 347, <https://doi.org/10.1038/s41597-022-01460-w>, 2022.
- 820

- Yin, Y., Chevallier, F., Ciais, P., Bousquet, P., Saunois, M., Zheng, B., Worden, J., Bloom, A. A., Parker, R. J., Jacob, D. J., Dlugokencky, E. J., and Frankenberg, C.: Accelerating methane growth rate from 2010 to 2017: leading contributions from the tropics and East Asia, *Atmospheric Chemistry and Physics*, 21, 12631–12647, <https://doi.org/10.5194/acp-21-12631-2021>, 2021.
- 825 Ying, Q., Poulter, B., Watts, J. D., Arndt, K. A., Virkkala, A.-M., Bruhwiler, L., Oh, Y., Rogers, B. M., Natali, S. M., Sullivan, H., Schiferl, L. D., Elder, C., Peltola, O., Bartsch, A., Armstrong, A., Desai, A. R., Euskirchen, E., Göckede, M., Lehner, B., Nilsson, M. B., Peichl, M., Sonnentag, O., Tuittila, E.-S., Sachs, T., Kalhori, A., Ueyama, M., and Zhang, Z.: WetCH<sub>4</sub>: A Machine Learning-based Upscaling of Methane Fluxes of Northern Wetlands during 2016–2022, *Earth System Science Data Discussions*, 2024, 1–45, <https://doi.org/10.5194/essd-2024-84>, 2024.
- 830 Yuan, K., Li, F., McNicol, G., Chen, M., Hoyt, A., Knox, S., Riley, W. J., Jackson, R., and Zhu, Q.: Boreal–Arctic wetland methane emissions modulated by warming and vegetation activity, *Nature Climate Change*, <https://doi.org/10.1038/s41558-024-01933-3>, 2024.
- Yvon-Durocher, G., Allen, A. P., Bastviken, D., Conrad, R., Gudas, C., St-Pierre, A., Thanh-Duc, N., and del Giorgio, P. A.: Methane fluxes show consistent temperature dependence across microbial to ecosystem scales, *Nature*, 507, 488–491, 835 <https://doi.org/10.1038/nature13164>, 2014.
- Zhang, Y., Jacob, D. J., Lu, X., Maasakkers, J. D., Scarpelli, T. R., Sheng, J.-X., Shen, L., Qu, Z., Sulprizio, M. P., Chang, J., Bloom, A. A., Ma, S., Worden, J., Parker, R. J., and Boesch, H.: Attribution of the accelerating increase in atmospheric methane during 2010–2018 by inverse analysis of GOSAT observations, *Atmospheric Chemistry and Physics*, 21, 3643–3666, <https://doi.org/10.5194/acp-21-3643-2021>, 2021b.
- 840 Zhang, Z., Poulter, B., Feldman, A. F., Ying, Q., Ciais, P., Peng, S., and Li, X.: Recent intensification of wetland methane feedback, *Nature Climate Change*, 430–433, <https://doi.org/10.1038/s41558-023-01629-0>, 2023a.
- Zhang, Z., Bansal, S., Chang, K.-Y., Fluet-Chouinard, E., Delwiche, K., Goeckede, M., Gustafson, A., Knox, S., Leppänen, A., Liu, L., Liu, J., Malhotra, A., Markkanen, T., McNicol, G., Melton, J. R., Miller, P. A., Peng, C., Raivonen, M., Riley, W. J., Sonnentag, O., Aalto, T., Vargas, R., Zhang, W., Zhu, Q., Zhu, Q., Zhuang, Q., Windham-Myers, L., Jackson, R. B., and 845 Poulter, B.: Characterizing Performance of Freshwater Wetland Methane Models Across Time Scales at FLUXNET-CH<sub>4</sub> Sites Using Wavelet Analyses, *Journal of Geophysical Research: Biogeosciences*, 128, e2022JG007259, <https://doi.org/10.1029/2022JG007259>, 2023b.
- Zhang, Z., Fluet-Chouinard, E., Jensen, K., McDonald, K., Hugelius, G., Gumbrecht, T., Carroll, M., Prigent, C., Bartsch, A., and Poulter, B.: Development of the global dataset of Wetland Area and Dynamics for Methane Modeling (WAD2M), *Earth 850 System Science Data*, 13, 2001–2023, <https://doi.org/10.5194/essd-13-2001-2021>, 2021a.
- Zhang, Z., Poulter, B., Knox, S., Stavert, A., McNicol, G., Fluet-Chouinard, E., Feinberg, A., Zhao (赵园红), Y., Bousquet,

- P., Canadell, J. G., Ganesan, A., Hugelius, G., Hurtt, G., Jackson, R. B., Patra, P. K., Saunio, M., Höglund-Isaksson, L., Huang (黄春林), C., Chatterjee, A., and Li (李新), X.: Anthropogenic emission is the main contributor to the rise of atmospheric methane during 1993–2017, *National Science Review*, nwab200, <https://doi.org/10.1093/nsr/nwab200>, 2021c.
- 855 Zhang, Z., Zimmermann, N. E., Calle, L., Hurtt, G., Chatterjee, A., and Poulter, B.: Enhanced response of global wetland methane emissions to the 2015–2016 El Niño-Southern Oscillation event, *Environmental Research Letters*, 13, 074009, <https://doi.org/10.1088/1748-9326/aac939>, 2018.
- Zhang, Z., Zimmermann, N. E., Stenke, A., Li, X., Hodson, E. L., Zhu, G., Huang, C., and Poulter, B.: Emerging role of wetland methane emissions in driving 21st century climate change, *Proceedings of the National Academy of Sciences*, 114, 860 9647–9652, <https://doi.org/10.1073/pnas.1618765114>, 2017.
- Zhu, Q., Peng, C., Ciais, P., Jiang, H., Liu, J., Bousquet, P., Li, S., Chang, J., Fang, X., Zhou, X., Chen, H., Liu, S., Lin, G., Gong, P., Wang, M., Wang, H., Xiang, W., and Chen, J.: Interannual variation in methane emissions from tropical wetlands triggered by repeated El Niño Southern Oscillation, *Global Change Biology*, 23, 4706–4716, <https://doi.org/10.1111/gcb.13726>, 2017.
- 865 Zona, D., Gioli, B., Commane, R., Lindaas, J., Wofsy, S. C., Miller, C. E., Dinardo, S. J., Dengel, S., Sweeney, C., Karion, A., Chang, R. Y.-W., Henderson, J. M., Murphy, P. C., Goodrich, J. P., Moreaux, V., Liljedahl, A., Watts, J. D., Kimball, J. S., Lipson, D. A., and Oechel, W. C.: Cold season emissions dominate the Arctic tundra methane budget, *Proceedings of the National Academy of Sciences*, 113, 40–45, <https://doi.org/10.1073/pnas.1516017113>, 2016.